Hybrid Beamforming and Adaptive RF Chain Activation for Uplink Cell-Free Millimeter-Wave Massive MIMO Systems

Nhan Thanh Nguyen, Kyungchun Lee, *Senior Member, IEEE*, and Huaiyu Dai, *Fellow, IEEE*,

Abstract

In this work, we investigate hybrid analog-digital beamforming (HBF) architectures for uplink cell-free (CF) millimeter-wave (mmWave) massive multiple-input multiple-output (MIMO) systems. We first propose two HBF schemes, namely, centralized HBF (C-HBF) and semi-centralized HBF (SC-HBF) with the assumptions of a capacity-achieving advanced receiver for digital processing and perfect channel state information (CSI) at the access points (APs). For analog processing, in C-HBF, the analog beamforming matrix is generated at the central processing unit (CPU) based on the CSI received from all APs, whereas that in SC-HBF is generated independently at each AP based on the local CSI. We show that the SC-HBF scheme can achieve approximately the same total achievable rate as that given by the C-HBF scheme with lower computational complexity and no global CSI. Furthermore, to reduce the power consumption, we propose a novel adaptive radio frequency (RF) chain-activation (ARFA) scheme, which dynamically activates/deactivates RF chains and their connected analog-to-digital converters (ADCs) and phase shifters at the APs based on the CSI. For the activation of RF chains, four low-complexity algorithms are proposed, which can achieve up to 236% improvement in energy efficiency (EE) with only a marginal loss in the total achievable rate.

Index Terms

Cell-free massive MIMO, mmWave communication, hybrid beamforming, RF chain activation.

N. T. Nguyen and K. Lee are with the Department of Electrical and Information Engineering and the Research Center for Electrical and Information Technology, Seoul National University of Science and Technology, 232 Gongneung-ro, Nowon-gu, Seoul, 01811, Republic of Korea (e-mail: nhan.nguyen, kclee@seoultech.ac.kr).

H. Dai is with the Department of Electrical and Computer Engineering, North Carolina State University, NC, USA. (e-mail: Huaiyu_Dai@ncsu.edu).

I. Introduction

Recently, many attempts have been made to utilize millimeter waves (mmWaves) for high-datarate mobile broadband communications. The main challenge of mmWave communication is the large path loss due to high carrier frequencies, which significantly limits the system performance and cell coverage [1], [2]. Fortunately, the short wavelength of mmWave systems facilitates the deployment of massive multiple-input multiple-output (MIMO) systems, which can provide large beamforming gains to compensate for the path loss in mmWave channels. Furthermore, Ngo et al. in [3], [4] introduce a cell-free (CF) massive MIMO architecture, in which a very large number of distributed access points (APs) connected to a single central processing unit (CPU) simultaneously serve a much smaller number of users over the same time/frequency resources. Therefore, the CF massive MIMO system is capable of providing good quality of service (QoS) uniformly to all served users, regardless of their locations in the coverage area, by using simple linear signal processing schemes [3]–[5]. From these aspects, the combination of mmWave and CF massive MIMO systems with the deployment of large numbers of antennas at the APs could be a symbiotic convergence of technologies that can significantly improve the performance of next-generation wireless communication systems [5].

A. Related works

The performance CF massive MIMO systems in conventional sub-6-GHz frequency bands have been analyzed intensively [3], [4], [6]–[20]. In particular, the closed-form expression of the achievable rate of CF massive MIMO systems is derived in [3], [4], [6], [7]. Furthermore, comparisons of CF massive MIMO and conventional small-cell MIMO systems in [3], [4], [7]–[9] show that the former is more robust to shadow fading correlation and significantly outperforms the latter in terms of throughput and coverage probability. In [10], a low-complexity power control technique with zero-forcing (ZF) precoding design is introduced for CF massive MIMO systems. In [11], an optimal power-allocation algorithm is proposed to maximize the total EE, which can double the total EE compared to the equal power control scheme. Furthermore, an AP selection (APS) scheme is proposed in [11], in which each user chooses and connects to only a subset of APs to reduce the power consumption caused by the backhaul links. Meanwhile, in [12], the EE maximization problem is considered under the effect of quantization distortion of the weighted received signals at the APs. In [13], [14], the authors propose AP-clustering approaches to overcome limitations upon the scalability of CF massive MIMO systems. Specifically, the

APs are grouped in clusters and multiple CPUs are used to manage these clusters, leading to a reduction in the data distribution and computational complexity involved in channel estimation, power control, and beamforming.

Another line of work has attempted to investigate the performance of CF massive MIMO systems in mmWave channels [5], [21]–[23]. In particular, Femenias et al. introduced a hybrid beamforming (HBF) framework for CF mmWave massive MIMO systems with limited fronthaul capacity in [5], and the eigen-beamforming scheme is applied to generate precoders/combiners. Specifically, the phases of analog beamformers are obtained by quantizing those of dominant eigenvectors of the channel covariance matrix known at the APs. In [21], a hybrid precoding algorithm leveraging antenna-array response vectors is applied to distributed MIMO systems with partially-connected HBF architecture. Although the partially-connected HBF structure has lower power consumption than the fully-connected one, it cannot fully exploit the beamforming gains [24]. In [22] and [23], Alonzo et al. introduce an uplink multi-user estimation scheme along with low-complexity HBF architectures. Specifically, the baseband and analog precoders at each AP are generated by decomposing the fully digital ZF precoding matrix using the block-coordinate descent algorithm. Moreover, the problems of pilot assignment and channel estimation are considered in [25] and [26], respectively.

In mmWave communications, a large number of antennas at the APs not only provide beamforming gains to compensate for the propagation loss in mmWave channels, but also enhance favorable propagation [27]. In particular, it is shown, in [27], that given a fixed total number of antennas at the APs, using more antennas at fewer APs is more beneficial than deploying more APs with fewer antennas in terms of favorable propagation and channel hardening. However, an excessively large amount of power can be consumed in this deployment because signal processing in the conventional digital domain requires a dedicated RF chain and analog-to-digital converter (ADC) for each antenna. Therefore, energy-efficient HBF schemes dedicated to CF mmWave massive MIMO systems are required, but only limited works exist in the literature focusing on the optimization of HBF for CF mmWave massive MIMO systems. Specifically, in [5], [21]–[23], the analog beamformers are all separately generated at the APs based on the local CSI, which are similar to HBF schemes for small-cell mmWave massive MIMO systems when each AP in the CF mmWave massive MIMO system is considered as a base station in the small-cell system. The antenna-selection (AS) schemes, which are proposed for the transceiver with a limited number of RF chains in [28], [29], can be applied to CF mmWave massive MIMO systems to reduce

power consumption. However, they can cause performance degradation, especially for HBF in the highly correlated channels of mmWave communication [30].

B. Contributions

In this work, we investigate the HBF for uplink CF mmWave massive MIMO systems in two scenarios: the global CSI of all APs is available or unavailable at the CPU. Then, we propose an adaptive RF chain-activation (ARFA) scheme, which provides considerable power reduction while nearly maintaining the system's total achievable rate; thus, the EE is remarkably improved. Our specific contributions can be summarized as follows:

- We first propose the centralized HBF (C-HBF) and semi-centralized HBF (SC-HBF) schemes, in which the analog beamforming matrices for all APs are generated at the CPU based on the global CSI and at each AP based only on the local CSI, respectively. By exploiting the global CSI to jointly optimize the analog combiners at the CPU, C-HBF is expected to outperform SC-HBF. However, our analytical and numerical results show that SC-HBF can approximately achieve the performance of C-HBF while requiring substantially lower computational complexity and no global CSI.
- In CF mmWave massive MIMO systems with L APs and N RF chains at each AP, the power consumption is approximately proportional to LN. Because L is large in CF massive MIMO systems, the total power consumption can be excessively high. To overcome this challenge, we propose an ARFA scheme. In this scheme, the RF chains are selectively activated at the APs based on CSI, and the number of active RF chains at the APs is optimized so that the proposed scheme can significantly reduce the total power consumption while causing only marginal performance loss. Our numerical analysis reveals that in CF mmWave massive MIMO systems, the proposed ARFA scheme with a relatively small number of active RF chains can exhibit performance comparable to that of the conventional fixed-activation HBF scheme, which activates all the available RF chains. As a result, a considerable improvement in the EE is achieved.
- In the proposed ARFA scheme, high computational complexity is required to find the optimal numbers of active RF chains at numerous APs with an exhaustive search. To reduce complexity, we propose two low-complexity near-optimal algorithms for the ARFA with C-HBF aided by the tabu search and a fast search method, respectively. Furthermore, ARFA is incorporated with SC-HBF in the proposed SC-ARFA schemes, creating a singular value-based and path loss-based SC-ARFA wherein the CPU requires a very limited amount of

information from the APs. Our simulation results show that the proposed algorithms perform very close to the conventional HBF scheme, in which all the available RF chains are turned on.

We note that an RF chain-selection (RFS) scheme is introduced in [31] for the conventional small-cell mmWave massive MIMO system. The RFS scheme and our proposed ARFA scheme are similar in exploiting a reduced number of RF chains for power reduction. However, the contributions in our work are novel in the following aspects. First, the number of active RF chains at the base station in the conventional small-cell system, which is a single integer, is optimized in the RFS scheme by solving the EE-optimization problem [31]. In contrast, we consider the CF mmWave massive MIMO system, and the numbers of active RF chains at numerous APs are jointly optimized by maximizing the system's total achievable throughput. This results in unequal numbers of active RF chains at the APs, and an AP can even deactivate all RF chains, leading to significant power reduction. Second, [31] focuses on optimizing the number of RF chains at the transmitter rather than at the receiver to avoid the nontrivial integer programming problem. Our work fills in this hole by optimizing the numbers of active RF chains at the receivers, which are the APs in the uplink of CF mmWave massive MIMO systems. Because of these systematic differences, the algorithm presented in [31] cannot be leveraged for our proposed ARFA scheme, which thus requires novel algorithms as presented in Section IV.

The remainder of this paper is organized as follows: Section II introduces the system and channel models, whereas Section III describes the C-HBF and SC-HBF schemes. In Section IV, three low-complexity ARFA algorithms are presented and the power consumption of the proposed ARFA scheme is analyzed. Section V presents simulation results, and the conclusion follows in Section VI.

II. SYSTEM AND CHANNEL MODEL

A. System model

We consider the uplink of a CF mmWave massive MIMO system, where L APs and K user equipments (UEs) are distributed in a large area. Each AP is equipped with N_r receive antennas and $N(\leq N_r)$ RF chains, whereas each UE is equipped with N_t transmit antennas. All APs, which are connected to a CPU via fronthaul links, simultaneously and jointly serve K UEs. In the case where numerous antennas are used at the UEs, i.e., N_t is large, a hybrid precoding architecture can be employed to reduce the power consumption and hardware cost. However, in

this work, to focus on the design of the hybrid combiner at the receiver side, we assume that N_t is small, and a fully digital precoder is used at the UEs. In contrast, at the receiver side, baseband processing of the received signals is performed at the CPU, whereas RF processing, including operations on ADCs, RF chains, and phase shifters, is carried out at the APs. Furthermore, a fully-connected architecture is considered for analog combining, in which N RF chains are connected to N_r receive antennas via a network of NN_r phase shifters [32], [33]. To focus on analog processing, we assume that the signals processed by the analog combiner are passed through a capacity-achieving advanced digital receiver [24] at the CPU, such as sphere decoding [34] and tabu search [35], [36]. We adopt a narrowband block-fading channel model [32], [33] in which the analog-combined signal at the lth AP can be expressed as

$$\mathbf{y}_{l} = \sqrt{\rho} \sum_{k=1}^{K} \mathbf{F}_{l}^{H} \mathbf{H}_{kl} \mathbf{x}_{k} + \mathbf{F}_{l}^{H} \mathbf{z}_{l}, \tag{1}$$

where $\mathbf{x}_k \in \mathbb{C}^{N_t \times 1}$ is the vector of symbols sent from the kth UE such that $\mathbb{E}\left\{\mathbf{x}_k^H\mathbf{x}_k\right\} = 1, \forall k$, and $\mathbf{z}_l \in \mathbb{C}^{N_r \times 1}$ is a vector of independent and identically distributed (i.i.d.) samples of additive white Gaussian noise (AWGN), whereas the elements of \mathbf{z}_l have a distribution of $\mathcal{CN}(0, N_0)$. Furthermore, $\mathbf{H}_{kl} \in \mathbb{C}^{N_r \times N_t}$ denotes the channel matrix representing channels between the kth UE and lth AP, and ρ represents the average transmit power. The analog combining matrix at the lth AP, i.e., $\mathbf{F}_l \in \mathbb{C}^{N_r \times N}$, is given by $\mathbf{F}_l = [\mathbf{f}_{l1}, \dots, \mathbf{f}_{lN}]$, where $\mathbf{f}_{ln} = [\mathbf{f}_{ln}^{(1)}, \dots, \mathbf{f}_{ln}^{(N_r)}]^T$ is the analog weight vector corresponding to the nth RF chain at the lth AP, and $\mathbf{f}_{ln}^{(i)}$ is the ith element of \mathbf{f}_{ln} , which has the constant amplitude $1/\sqrt{N_r}$ but different phases, i.e., $\mathbf{f}_{ln}^{(i)} = \frac{1}{\sqrt{N_r}}e^{j\theta_{ln}^{(i)}}, \forall l, n, i$.

The composite received signal available at the CPU can be expressed as

$$\begin{bmatrix} \mathbf{y}_1 \\ \vdots \\ \mathbf{y}_L \end{bmatrix} = \sqrt{\rho} \sum_{k=1}^K \begin{bmatrix} \mathbf{F}_1^H \mathbf{H}_{k1} \\ \vdots \\ \mathbf{F}_L^H \mathbf{H}_{kL} \end{bmatrix} \mathbf{x}_k + \begin{bmatrix} \mathbf{F}_1^H \mathbf{z}_1 \\ \vdots \\ \mathbf{F}_L^H \mathbf{z}_L \end{bmatrix}. \tag{2}$$

Let $\mathbf{F} = \operatorname{diag} \{ \mathbf{F}_1, \dots, \mathbf{F}_L \} \in \mathbb{C}^{LN_r \times LN}$ be a block-diagonal matrix containing the analog combiners for all L APs. In this work, we refer to \mathbf{F} as the *global combiner*, whereas $\{ \mathbf{F}_1, \dots, \mathbf{F}_L \}$ for analog signal combining at the APs $\{1, \dots, L\}$ are referred to as the *local combiners*. Furthermore, let $\mathbf{H}_l = [\mathbf{H}_{1l}, \dots, \mathbf{H}_{Kl}] \in \mathbb{C}^{N_r \times KN_t}$ denote the channel matrix between the K UEs and lth AP, and define

$$egin{aligned} oldsymbol{y} &= egin{bmatrix} oldsymbol{y}_1 \ dots \ oldsymbol{y}_L \end{bmatrix}, \ oldsymbol{x} &= egin{bmatrix} oldsymbol{x}_1 \ dots \ oldsymbol{x}_K \end{bmatrix}, \ oldsymbol{z} &= egin{bmatrix} oldsymbol{z}_1 \ dots \ oldsymbol{z}_L \end{bmatrix}, \ oldsymbol{H} &= egin{bmatrix} oldsymbol{H}_1 \ dots \ oldsymbol{H}_L \end{bmatrix}, \end{aligned}$$

where $\mathbf{y} \in \mathbb{C}^{LN \times 1}$, $\mathbf{x} \in \mathbb{C}^{KN_t \times 1}$, $\mathbf{z} \in \mathbb{C}^{LN_r \times 1}$, and $\mathbf{H} \in \mathbb{C}^{LN_r \times KN_t}$. Then, (2) can be rewritten in a more compact form as

$$\mathbf{y} = \sqrt{\rho} \mathbf{F}^H \mathbf{H} \mathbf{x} + \mathbf{F}^H \mathbf{z}. \tag{3}$$

We note that the analog processing is separately performed at the APs because the ADCs, RF chains, and phase shifters are installed at the APs. However, $\{F_1, \ldots, F_L\}$ can be generated either at the APs based on their local CSI or at the CPU based on the global CSI. In this work, we refer to the former as the SC-HBF scheme and the latter as the C-HBF scheme. For the design and optimization of the analog beamformer in terms of both spectral and energy efficiencies, we assume that perfect CSI is available.

B. Channel model

The channels between the UEs and APs are modeled based on the geometric Saleh–Valenzuela channel model, which is a typical channel model for mmWave systems [37], [38]. Specifically, the channel matrix between the *l*th AP and *k*th UE can be expressed as [33]

$$\boldsymbol{H}_{kl} = \sqrt{\frac{G_a}{\beta_{kl}} \frac{N_r N_t}{P_{kl}}} \sum_{p=1}^{P_{kl}} \alpha_{kl}^{(p)} \boldsymbol{a}_r(\phi_{kl}^{(p)}) \boldsymbol{a}_t^H(\psi_{kl}^{(p)}), \tag{4}$$

where P_{kl} is the number of effective channel paths corresponding to a limited number of scatters between the kth UE and the lth AP, $\alpha_{kl}^{(p)}$ is the gain of the pth path. Furthermore, $\phi_{kl}^{(p)}$ and $\psi_{kl}^{(p)}$ are the azimuth angles of arrival (AoA) and departure (AoD), respectively. All channel path gains $\alpha_{kl}^{(p)}$ are assumed to be i.i.d. Gaussian random variables with zero mean and unit variance, i.e., $\alpha_{kl}^{(p)} \sim \mathcal{CN}(0,1), \forall l,k$. Furthermore, $a_r(\cdot)$ and $a_t(\cdot)$ represent the normalized receive and transmit array response vectors at an AP and a UE, respectively, which depend on the structure of the antenna array. In this work, we consider a uniform linear array (ULA), where $a_r(\cdot)$ is given by $a_r(\phi) = \frac{1}{\sqrt{N_r}} [1, e^{j\frac{2\pi}{\lambda} d_s \sin(\phi)}, \dots, e^{j(N_r-1)\frac{2\pi}{\lambda} d_s \sin(\phi)}]^T$ with λ denoting the wavelength of the signal and d_s being the antenna spacing in the antenna array [33]. For the transmitter, $a_t(\cdot)$ can be written in a similar fashion. In (4), G_a is the total antenna gain. Furthermore, β_{kl} represents the path loss between the kth UE and lth AP, which is given in dB as [39], [40]

$$\beta_{kl}[d\mathbf{B}] = \beta_0 + 10\epsilon \log_{10} \left(\frac{d_{kl}}{d_0}\right) + A_{\xi}.$$
 (5)

Here, $\beta_0 = 10 \log_{10} \left(\frac{4\pi d_0}{\lambda}\right)^2$, where $d_0 = 1$ m, ϵ is the average path loss exponent over distance, and A_{ξ} is a zero-mean Gaussian random variable with a standard deviation ξ in dB representing the effect of shadow fading.

III. C-HBF AND SC-HBF

A. C-HBF

For simplification, we assume $F_l^H F_l \approx I_N$ [32], [41], which is tight in the considered CF mmWave massive MIMO system with a sufficiently large number of antennas being deployed at each AP. Under this assumption, the noise covariance matrix after analog combining can be given as $\mathbf{R} = N_0 \mathbf{F}^H \mathbf{F} \approx N_0 \mathbf{I}_{LN}$, which is still approximately white Gaussian noise. This simplifies the expression of the total achievable rate and facilitates the subsequent analysis and optimization. Specifically, the total achievable rate R for the analog-combined signal in (3) can be expressed as [32]

$$R = \log_2 \det \left(\mathbf{I}_{LN} + \rho \mathbf{R}^{-1} \mathbf{F}^H \mathbf{H} \mathbf{H}^H \mathbf{F} \right) \approx \log_2 \det \left(\underbrace{\mathbf{I}_{KN_t} + \gamma \mathbf{H}^H \mathbf{F} \mathbf{F}^H \mathbf{H}}_{\triangleq \boldsymbol{\varrho}} \right), \tag{6}$$

where $\gamma = \frac{\rho}{N_0}$. In the following theorem, we show that R can be expressed as the sum of L sub-rates corresponding to L APs.

Theorem 1: In a CF mmWave massive MIMO system with L APs, the total achievable rate can be expressed as

$$R = \sum_{l=1}^{L} R_l, \tag{7}$$

where R_l is the sub-rate corresponding to the lth AP, given as

$$R_{l} = \log_{2} \det \left(\mathbf{I}_{N} + \gamma \mathbf{F}_{l}^{H} \mathbf{H}_{l} \mathbf{Q}_{l-1}^{-1} \mathbf{H}_{l}^{H} \mathbf{F}_{l} \right), \tag{8}$$

with $\boldsymbol{Q}_0 = \boldsymbol{I}_{KN_t}$ and

$$Q_{l-1} = Q_{l-2} + \gamma H_{l-1}^H F_{l-1} F_{l-1}^H H_{l-1}.$$
(9)

Proof: See Appendix A.

The optimal global analog combiner is the solution to the problem of optimizing the total achievable rate, which can be formulated as

$$F^* = \arg \max_{\mathbf{F}} R, \quad \text{s.t. } F = \operatorname{diag} \{F_1, \dots, F_L\} \text{ and } f_{ln} \in \mathcal{F}, \forall l, n,$$
 (10)

where \mathcal{F} is the set of feasible analog combiners. Based on Theorem 1, the total achievable rate R can be maximized by optimizing sub-rates $\{R_1, \ldots, R_L\}$ corresponding to APs $\{1, \ldots, L\}$.

Algorithm 1 C-HBF scheme

```
Output: F^* and \{R_1, R_2, ..., R_L\}.
  1: Q_0 = I_K
  2: for l=1 \rightarrow L do
              for n=1 \to N do
                     Set u_{ln}^{\star} to the singular vector corresponding to the nth largest singular value of H_l Q_{l-1}^{-1} H_l^H.
  4:
                   f_{ln}^{\star} = \frac{1}{\sqrt{N_n}} \mathcal{Q}(\boldsymbol{u}_{ln}^{\star})
  5:
              end for
  6:
            oldsymbol{F}_l^\star = [oldsymbol{f}_{l1}^\star, \dots, oldsymbol{f}_{lN}^\star]
            \boldsymbol{G}_{l} = \boldsymbol{H}_{l}^{H} \boldsymbol{F}_{l}^{\star} \boldsymbol{F}_{l}^{\star H} \boldsymbol{H}_{l}
  9: \mathbf{Q}_l = \mathbf{Q}_{l-1} + \gamma \mathbf{G}_l
10: R_l = \log_2 \left( \boldsymbol{I}_N + \gamma \boldsymbol{F}_l^{\star H} \boldsymbol{H}_l \boldsymbol{Q}_{l-1}^{-1} \boldsymbol{H}_l^H \boldsymbol{F}_l^{\star} \right)
11: end for
12: F^* = \text{diag}\{F_1^*, \dots, F_L^*\}
```

As a result, finding the optimal global combiner F^* in (10) can be factorized into finding the optimal local combiners:

$$\boldsymbol{F}_{l}^{\star} = \arg \max_{\boldsymbol{F}_{l}} R_{l}, \forall l, \quad \text{s.t.} \quad \boldsymbol{f}_{l1}, \dots, \boldsymbol{f}_{lN} \in \mathcal{F}$$
 (11)

Let $\{u_{l1}^{\star}, \ldots, u_{lN}^{\star}\}$ be the N singular vectors corresponding to N largest singular values of $H_l Q_{l-1}^{-1} H_l^H$, which are in decreasing order. Then, columns $\{f_{l1}^{\star}, \ldots, f_{lN}^{\star}\}$ of a near-optimal solution to (11) can be obtained by quantizing $\{u_{l1}^{\star}, \ldots, u_{lN}^{\star}\}$, respectively, to the nearest vector in \mathcal{F} [21], i.e.,

$$\boldsymbol{f}_{ln}^{\star} = \arg\min_{\boldsymbol{f}_{ln} \in \mathcal{F}} \|\boldsymbol{u}_{ln}^{\star} - \boldsymbol{f}_{ln}\|^{2}, \forall n.$$
 (12)

It is evident from (8) and (9) that R_l depends not only on \mathbf{H}_l , but also on $\mathbf{H}_{l-1}, \mathbf{H}_{l-2}, \dots, \mathbf{H}_1$. Therefore, from (8) and (11), it is observed that finding \mathbf{F}_l^{\star} requires not only \mathbf{H}_l but also $\mathbf{H}_{l-1}, \mathbf{H}_{l-2}, \dots, \mathbf{H}_1$. This is similar to the requirements for determining analog beamformers for sub-arrays in the partially-connected HBF architecture [24], [42]. As a result, solving $\mathbf{F}^{\star} = [\mathbf{F}_1^{\star}, \mathbf{F}_2^{\star}, \dots, \mathbf{F}_L^{\star}]$ requires the CSI of the channels between all L APs and K UEs, i.e., $\{\mathbf{H}_1, \mathbf{H}_2, \dots, \mathbf{H}_L\}$, which can be available at the CPU; hence, finding \mathbf{F}^{\star} based on (11) requires a C-HBF scheme.

Algorithm 1 presents the proposed C-HBF scheme to obtain F^* . In particular, in steps 3–6, the combining vector f_{ln}^* is obtained by quantizing \mathbf{u}_{ln}^* based on (12), which ensures that the resultant analog combiners belong to the feasible set \mathcal{F} . Then, F_l^* is found in step 7 and G_l is computed in step 8, followed by Q_l being updated in step 9 based on (9). In step 10, the

sub-rate R_l corresponding to the lth AP is computed. Finally, the global analog combiner F^* is determined in step 12.

B. SC-HBF

Let $\{\tilde{\boldsymbol{u}}_{l1}^{\star}, \dots, \tilde{\boldsymbol{u}}_{lN}^{\star}\}$ be the N singular vectors corresponding to the N largest singular values of \boldsymbol{H}_l , which are in decreasing order. Furthermore, define

$$\tilde{\boldsymbol{f}}_{ln}^{\star} = \arg\min_{\boldsymbol{f}_{ln} \in \mathcal{F}} \|\tilde{\boldsymbol{u}}_{ln}^{\star} - \boldsymbol{f}_{ln}\|^{2}, \forall n.$$
(13)

Then, in the SC-HBF scheme, the optimal local analog combiner generated at the lth AP based on \boldsymbol{H}_l can be given as $\tilde{\boldsymbol{F}}_l^{\star} = \left[\tilde{\boldsymbol{f}}_{l1}^{\star}, \ldots, \tilde{\boldsymbol{f}}_{lN}^{\star}\right]$ [21]. Let $\tilde{\boldsymbol{F}}^{\star} = \operatorname{diag}\left\{\tilde{\boldsymbol{F}}_1^{\star}, \ldots, \tilde{\boldsymbol{F}}_L^{\star}\right\}$. In the following theorem, we show that the SC-HBF scheme can approximately achieve the total achievable rate of the C-HBF scheme.

Theorem 2: In CF mmWave massive MIMO systems with large L and low SNRs due to the significant pathloss in the mmWave channels, the total achievable rate of the SC-HBF scheme, denoted by \tilde{R} , is approximately the same as that of the C-HBF scheme, i.e.,

$$\tilde{R} = \log_2 \det \left(\mathbf{I}_{KN_t} + \gamma \mathbf{H}^H \tilde{\mathbf{F}}^* \tilde{\mathbf{F}}^{*H} \mathbf{H} \right) \approx R,$$
 (14)

where R is given in (7).

It is observed that in the SC-HBF scheme, the local analog combiners are independently generated at the APs. As a result, the APs do not need to send their CSI to the CPU, and the CPU does not need to feed back the generated combining matrices to the APs, as in the C-HBF. Instead, only the information of the analog-combined channel matrix $F_l^H H_l$, whose dimension is substantially lower than that of the original channel matrix, needs to be sent to the CPU for digital processing. Moreover, SC-HBF can be performed with considerably lower computational complexity than C-HBF. Specifically, only N singular vectors corresponding to the N largest singular values of the channel matrix are required to form the analog combiner. In contrast, additional matrix inversions, multiplications, and additions are performed in steps 4, 8, and 9 of Algorithm 1 for the C-HBF scheme. Notably, despite the simpler implementation and lower complexity of the SC-HBF scheme, it can approximately achieve the performance of C-HBF, as stated in Theorem 2. This suggests that the generation of analog combiners can be conducted independently at the APs rather than at the CPU for complexity reduction as well as for reduced information exchange on the fronthaul links.

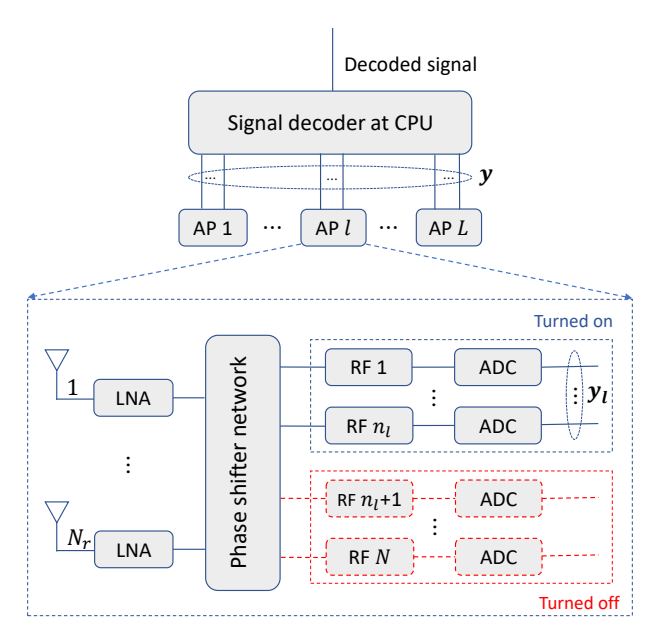


Fig. 1. HBF architecture with the ARFA scheme. In the phase-shifter network, $n_l N_r$ out of NN_r phase shifters are turned on at the lth AP.

We note that the term (semi-)centralized in our work implies the place where the analog combiners are generated rather than the level of receiver cooperation for decoding as in [9]. More specifically, in the fully centralized decoding scheme considered in [9], the pilot and data signals received at all APs are gathered at the CPU for data detection. In contrast, in the C-HBF scheme, the signal combining still needs to be conducted separately in two stages, i.e., analog combining at the AP and digital decoding at the CPU, because the phase shifters and RF chains are installed at the APs. Therefore, our finding in Theorem 2 is not against the conclusion in [9] regarding the performance comparison of centralized and local processing schemes in CF massive MIMO systems.

Theorem 2 indicates that the global CSI at the CPU is not very helpful in improving the achievable rate in CF mmWave massive MIMO systems. However, this does not mean that further information exchange via the fronthaul links is completely useless. Indeed, the information exchange between the APs and CPU in CF massive MIMO systems can also be exploited to improve the EE. In the next section, it is discussed that by adaptively activating RF chains based on global CSI in C-HBF or on limited information in SC-HBF, the power consumption can be reduced, which leads to improved EE.

IV. ADAPTIVE RF CHAIN ACTIVATION

A. Problem formulation and basic ideas

The global analog combiner F can be expressed as

$$extbf{\emph{F}} = ext{diag} \{ \underbrace{ \left[extbf{\emph{f}}_{11}, \ldots, extbf{\emph{f}}_{1N}
ight]}_{ ext{analog combiner at AP 1}}, \ldots, \underbrace{ \left[extbf{\emph{f}}_{L1}, \ldots, extbf{\emph{f}}_{LN}
ight]}_{ ext{analog combiner at AP } L} \},$$

and the following facts are noted:

- Based on Theorem 1, the total achievable rate can be expressed as a sum of sub-rates $\{R_1, \ldots, R_L\}$ corresponding to APs $\{1, \ldots, L\}$. In CF mmWave massive MIMO systems, the APs are distributed in a large area, and their communication channels experience different path losses and shadowing effects. Therefore, the contributions of the local analog combiners at different APs to the total achievable rate are of different significances.
- In a local analog combiner F_l , combining vectors $\{f_{l1}, \ldots, f_{lN}\}$ have different contributions to the sub-rate R_l given in (8). Specifically, the contribution of f_{ln} is more significant than that of f_{lm} if n < m because n and m are the indices of the ordered singular values of $H_l Q_{l-1}^{-1} H_l^H$ in C-HBF and of H_l in SC-HBF.

As a result, it is likely that a subset of analog combining vectors in $\{f_{11},\ldots,f_{LN}\}$ are insignificant and can be removed from the global combiner F without causing considerable performance loss. We note that at an AP, an analog combining vector represents the effect of N_r phase shifters connected to an RF chain, followed by an ADC. Therefore, an insignificant analog combining vector can be removed from signal combining by turning off its corresponding RF chain, ADC, and phase shifters, which results in a reduction in the total power consumption. Motivated by this, we propose an ARFA scheme that selectively activates RF chains at the APs. Let $\mathbf{n} = \{n_1, \ldots, n_L\}$, where n_l is the number of turned-on RF chains out of N RF chains installed at the lth AP, $0 \le n_l \le N$. We note that for $n_l = 0$, all the RF chains at the lth AP are turned off, and this AP does not consume any power for signal combining. The optimal activation of RF chains at the APs can be performed based on the following remark.

Remark 1: Because f_{ln} is always more important at the lth AP than f_{lm} with n < m in terms of achievable rate, the problem of optimal activation of RF chains at an AP is equivalent to finding an optimal number of turned-on RF chains at that AP. Specifically, for the lth AP, if the ARFA scheme suggests using n_l^* RF chains, then the first n_l^* RF chains corresponding to

 $\{f_{l1},\ldots,f_{ln_l^{\star}}\}$ are selected for analog signal combining, whereas the others are deactivated to save power.

The HBF architecture with the proposed ARFA scheme is illustrated in Fig. 1. As an example, at the lth AP, only n_l out of N RF chains are turned on. Furthermore, the ADCs and phase shifters connected to the inactive RF chains are also turned off. Consequently, the local combiner \mathbf{F}_l consists of only n_l analog combining vectors, i.e., $\mathbf{F}_l = \{\mathbf{f}_1, \dots, \mathbf{f}_{n_l}\}$.

Unlike the conventional fixed-activation HBF, in the proposed ARFA scheme, the global combiner F, sub-rate R_l , and achievable rate R depend on n. Therefore, in this section, they are expressed as functions of n, i.e., F(n), $R_l(n)$, and R(n), respectively. We limit the total number of turned-on RF chains in the ARFA scheme to $L\bar{n}$, i.e., $\sum_{l=1}^{L} n_l = L\bar{n}$, where $\bar{n} (\leq N)$ is the average number of activated RF chains at each AP. Based on Remark 1, the optimal activation of RF chains at the APs in the ARFA scheme can be performed by solving

$$\boldsymbol{n}^{\star} = \arg\max_{\boldsymbol{n} \in \mathcal{S}} R(\boldsymbol{n}), \tag{15}$$

where $S = \left\{ \boldsymbol{n} : 0 \leq n_l \leq N, \sum_{l=1}^L n_l = L\bar{n} \right\}$ is the feasible set of \boldsymbol{n} . The optimal \boldsymbol{n}^* in (15) can be found by exhaustive search over the entire feasible set S. However, in CF mmWave massive MIMO systems, L is large; thus, an excessively large number of candidates for \boldsymbol{n} need to be examined in the exhaustive search, which is almost computationally prohibitive. In the following subsections, we propose three low-complexity algorithms to find \boldsymbol{n}^* . By abuse of notation, we use \boldsymbol{F}^* for the global combiner found by the proposed ARFA algorithms. Furthermore, we note that Algorithm 1 can be easily modified for the ARFA scheme by replacing N in steps 3, 7, and 10 with n_l , reflecting a dynamic number of analog combining vectors for the local combiner \boldsymbol{F}_l at the lth AP.

B. ARFA with C-HBF (C-ARFA)

In C-ARFA, the ARFA scheme is incorporated with C-HBF, and the optimal numbers of active RF chains at the APs are found at the CPU based on the global CSI.

1) Tabu search (TS)-aided C-ARFA: The TS approach can find a near-optimal solution with reduced complexity compared to the exhaustive search. It is widely used for symbol detection in massive MIMO systems [35], [36]. In this section, we propose the TS-aided C-ARFA scheme, which is summarized in Algorithm 2.

In the TS-aided C-ARFA algorithm, candidates n and their neighbors are examined over a sufficiently large number of search iterations. The final output is the best solution found until

Algorithm 2 TS-aided C-ARFA scheme

```
Output: F^*
```

```
1: Initialize \mathbf{n} = [n_1, \dots, n_L] with n_l = \bar{n}, \forall l.
 2: Use Algorithm 1 to find F(\mathbf{n}), R_l(\mathbf{n}), \forall l, and R(\mathbf{n}) = \sum_{l=1}^L R_l(\mathbf{n}).
 3: \mathbf{F}^{\star} = \mathbf{F}(\mathbf{n}), R^{\star} = R(\mathbf{n})
 4: \bar{R} = \frac{R(\mathbf{n})}{L}, count = 0
 5: for iter = 1 \rightarrow \mathcal{I} do
             Find the neighbor set \mathcal{N}(\mathbf{n}) = {\hat{\mathbf{n}}_1, \hat{\mathbf{n}}_2, ...} of \mathbf{n} based on (16).
 6:
            Use Algorithm 1 to find F(\hat{\mathbf{n}}_i), R_l(\hat{\mathbf{n}}_i), \forall l, and R(\hat{\mathbf{n}}_i) = \sum_{l=1}^L R_l(\hat{\mathbf{n}}_i), i = 1, 2, ..., |\mathcal{N}(\mathbf{n})|.
 7:
            Find the best neighbor: \hat{\mathbf{n}}^* = \arg \max_{\hat{\mathbf{n}}_i \in \mathcal{N}(\mathbf{n})} R(\hat{\mathbf{n}}_i).
 8:
            if R(\hat{\boldsymbol{n}}^{\star}) > R^{\star} then
 9:
                  Update \mathbf{F}^{\star} = \mathbf{F}(\hat{\mathbf{n}}^{\star}) and set count = 0.
10:
            else
11:
12:
                  Update count = count + 1. Early terminate the search if count > count_{max}.
            end if
13:
            Push n to the tabu list \mathcal{T}.
14:
             Update \mathbf{n} = \hat{\mathbf{n}}^{\star}, R_l(\mathbf{n}) = R_l(\hat{\mathbf{n}}^{\star}), \forall l, and \bar{R} = \frac{R(\hat{\mathbf{n}}^{\star})}{L}.
15:
16: end for
```

the search is terminated. The iterative search process is first initialized in step 1, where all the elements of \mathbf{n} are set to \bar{n} . Then, Algorithm 1 is employed in step 2 to find $\mathbf{F}(\mathbf{n})$, $R_l(\mathbf{n})$, $\forall l$, and $R(\mathbf{n})$. In step 3, \mathbf{F}^* is initialized as $\mathbf{F}(\mathbf{n})$, and R^* is set to $R(\mathbf{n})$ as a threshold to determine whether a new candidate results in better performance.

The iterative search process is performed in steps 5–16. Specifically, a neighbor set $\mathcal{N}(\mathbf{n}) = \{\hat{\mathbf{n}}_1, \hat{\mathbf{n}}_2, \ldots\}$ of \mathbf{n} is found in step 6. Here, a neighbor is obtained by simultaneously increasing an element and decreasing another element of \mathbf{n} . To reduce the number of neighbors, which can be excessively large in CF massive MIMO systems, only more likely candidates are examined. Specifically, because more RF chains should typically be used at the APs with larger sub-rates, a neighbor of \mathbf{n} is obtained by decreasing n_i by one if $R_i(\mathbf{n}) < \bar{R}$, and increasing n_j by one if $R_j(\mathbf{n}) > \bar{R}$, with $i, j = 1, \ldots, L$, $i \neq j$, and \bar{R} computed in step 4. As a result, the neighbor set can be defined as

$$\mathcal{N}(\mathbf{n}) = \{ \hat{\mathbf{n}} \in \mathcal{S} \setminus \mathcal{T} : \hat{n}_i = n_i - 1 \text{ if } R_i(\mathbf{n}) < \bar{R}, \hat{n}_j = n_j + 1 \text{ if } R_j(\mathbf{n}) > \bar{R},$$

$$i, j = 1, \dots, L, i \neq j \}, \tag{16}$$

where \mathcal{T} represents a tabu list, which contains the visited candidates, and $\mathcal{S}\setminus\mathcal{T}$ is a subset containing non-tabu candidates in \mathcal{S} . Then, the neighbors are examined in step 7 to determine

Algorithm 3 FS-aided C-ARFA scheme

```
Output: F^*
```

```
1: Initialize \mathbf{n} = [n_1, \dots, n_L] with n_l = \bar{n}, \forall l.
 2: Use Algorithm 1 to find F(\mathbf{n}), R_l(\mathbf{n}), \forall l, and R(\mathbf{n}) = \sum_{l=1}^{L} R_l(\mathbf{n}).
 3: \mathbf{F}^* = \mathbf{F}(\mathbf{n}), R^* = R(\mathbf{n}).
 4: Obtain \{n_{[1]},\ldots,n_{[L]}\} s.t. R_{[1]}({\bf n})>\ldots>R_{[L]}({\bf n}).
 5: i = 1, k = L
 6: while i < k do
         while n_{[i]} = N do
 7:
             i = i + 1
 8:
         end while
 9:
         while n_{[k]} = 0 do
10:
             k = k - 1
11:
12:
         end while
13:
         Update n: n_{[i]} = n_{[i]} + 1, n_{[k]} = n_{[k]} - 1.
         Use Algorithm 1 to find F(n) and R(n) with the updated n.
14:
         Update \mathbf{F}^* = \mathbf{F}(\hat{\mathbf{n}}^*) if R(\hat{\mathbf{n}}^*) > R^*.
15:
16: end while
```

the best one, denoted by $\hat{\boldsymbol{n}}^{\star}$, in step 8. In step 10, \boldsymbol{F}^{\star} is updated if $\hat{\boldsymbol{n}}^{\star}$ results in better performance, which is determined by comparing $R(\hat{\boldsymbol{n}}^{\star})$ to R^{\star} in step 9. In step 15, \boldsymbol{n} , $R_l(\boldsymbol{n})$, $\forall l$, and \bar{R} are updated for the next search iteration. The search is terminated once the maximum number of iterations \mathcal{I} is reached or early termination occurs in step 12.

Although the TS-aided C-ARFA algorithm can provide near-optimal performance and requires lower complexity compared to that required by the exhaustive search, its computational complexity can be still high when L is large. In the next section, we propose a fast search algorithm to further reduce complexity with only a marginal performance loss with respect to the TS-aided C-ARFA scheme.

2) Fast search (FS)-aided C-ARFA: The idea of the FS-aided C-ARFA scheme is to turn on/off as many RF chains as possible at the APs corresponding to the largest/smallest sub-rates R_l , as presented in Algorithm 3. In steps 1–3, all elements of \mathbf{n} are set to \bar{n} , then $\mathbf{F}(\mathbf{n})$, $R_l(\mathbf{n})$, $\forall l$, and $R(\mathbf{n})$ are computed. In step 4, the elements of \mathbf{n} are ordered to obtain $\{n_{[1]}, \ldots, n_{[L]}\}$ in the decreasing order of sub-rates $\{R_1(\mathbf{n}), \ldots, R_L(\mathbf{n})\}$. Therefore, $n_{[i]}$ is the number of turned-on RF chains at the AP with the ith largest sub-rates, i.e., $R_{[i]}(\mathbf{n})$.

In step 5, we initialize i = 1 and k = L. In steps 6–16, $n_{[i]}$ is increased by one, whereas

 $n_{[k]}$ is decreased by one, in each iteration. We note that in step 13, $n_{[i]}$ and $n_{[k]}$ are updated simultaneously to guarantee $\sum_{l=1}^{L} n_{[l]} = L\bar{n}$. The updates of $n_{[i]}$ and $n_{[k]}$ result in a new candidate \mathbf{n} . Hence, $\mathbf{F}(\mathbf{n})$ and $R(\mathbf{n})$ are found in step 14, and \mathbf{F}^{\star} is updated if the performance is improved, as shown in step 15. Once $n_{[i]}$ reaches the maximum, i.e., N, the number of turned-on RF chains at the AP associated with the (i+1)th largest sub-rate, i.e., $n_{[i+1]}$, is considered, as shown in steps 7–9. In contrast, if $n_{[k]}$ reaches the minimum, i.e., zero, $n_{[k-1]}$ is considered next, as shown in steps 10–12. This iterative process is terminated if $i \geq k$, for which we have $R_{[i]}(\mathbf{n}) \leq R_{[k]}(\mathbf{n})$ and the increase (decrease) in $n_{[i]}$ ($n_{[k]}$) is unlikely to provide performance improvement.

We note that the ARFA process needs to be performed at the CPU to jointly optimize the numbers of RF chains at all APs. In the TS- and FS-aided C-ARFA schemes, the global CSI is exploited to evaluate the candidates for *n*. However, the employment of C-HBF in these schemes requires high computational complexity and a large amount of information exchanged between the CPU and APs, as discussed in Section III-B. This motivates us to propose an ARFA scheme incorporated with SC-HBF in the next subsection.

C. ARFA with SC-HBF (SC-ARFA)

Without global CSI, the ARFA scheme can be performed if the CPU knows the qualities of the available combining vectors or the path loss corresponding to each AP. The former idea relies on the fact that a combining vector is obtained by quantizing a singular vector of the channel matrix, as shown in (13). Therefore, the quality of a combining vector can be evaluated based on its corresponding singular value. In contrast, the latter idea for SC-ARFA is motivated by the observation that the AP with more significant path loss should have fewer activated RF chains because it is more likely to have a low sub-rate. This scheme exhibits performance loss but requires lower fronthauling loads than the former.

1) Singular values-based SC-ARFA (SV-based SC-ARFA): The SV-based SC-ARFA scheme is summarized in Algorithm 4. Specifically, in step 1, each AP finds and sends the N largest singular values of the channel matrix to the CPU. Here, only the N largest singular values are sent because, in the proposed ARFA scheme, only n_l out of N combining vectors are selected for signal combining at the lth AP. As a result, the set of LN singular values $\left\{\lambda_1^{(1)},\ldots,\lambda_N^{(1)},\ldots,\lambda_N^{(L)},\ldots,\lambda_N^{(L)},\ldots,\lambda_N^{(L)}\right\}$ is available at the CPU, with $\lambda_n^{(l)}$ being the nth largest singular value associated with the lth AP. Then, the numbers of active RF chains at the APs are determined in steps 3–6. Specifically, an RF chain at an AP is suggested for activation if its corresponding singular value is not smaller

Algorithm 4 Analog combining with SV-based SC-ARFA

Output: F^*

- 1: Each AP finds the N largest singular values of its channel matrix and sends them to the CPU. Specifically, the lth AP finds and sends to the CPU a vector $\mathbf{e}_l = \left[\lambda_1^{(l)}, \dots, \lambda_N^{(l)}\right]$, with $\lambda_n^{(l)}$ being the nth largest singular value of \mathbf{H}_l .
- 2: The CPU finds $\lambda_{L\bar{n}}$, which is the $(L\bar{n})$ th largest element in the singular value set $\{\lambda_1^{(1)},\ldots,\lambda_N^{(1)},\ldots,\lambda_1^{(L)},\ldots,\lambda_N^{(L)}\}$ received from all APs.
- 3: for $l=1 \rightarrow L$ do
- 4: The CPU sets n_l^{\star} to the number of elements in e_l that are not smaller than $\lambda_{L\bar{n}}$ and sends n_l^{\star} to the lth AP.
- 5: The *l*th AP determines its local analog combiner F_l^{\star} for n_l^{\star} RF chains, i.e., $F_l^{\star} = [\tilde{f}_{l1}^{\star}, \dots, \tilde{f}_{ln_l^{\star}}^{\star}]$, where \tilde{f}_{ln}^{\star} is given by (13).

6: end for

than $\lambda_{L\bar{n}}$ found in step 2. In other words, the number of active RF chains at the lth AP, i.e., n_l^{\star} , is set to the number of elements in $\left\{\lambda_1^{(l)},\ldots,\lambda_N^{(l)}\right\}$ that are not smaller than $\lambda_{L\bar{n}}$. Finally, the CPU sends the value n_l^{\star} back to the lth AP, which is then used for signal combining based on the SC-HBF scheme.

2) Path loss-based SC-ARFA (PL-based SC-ARFA): Let $\beta_l = \sum_{k=1}^K \beta_{kl}$ be the sum of path loss of the lth AP, with β_{kl} given in (5), and let $\alpha_l = \frac{1}{\beta_l}, \forall l$. The number of activated RF chains at the lth AP can be set to

$$n_l = \min \left\{ N, \left\lfloor L\bar{n} \frac{\alpha_l}{\sum_{i=1}^L \alpha_i} \right\rfloor \right\}, \forall l, \tag{17}$$

where $\min\{N,\cdot\}$ is used to guarantee $n_l \leq N$, and $\lfloor \cdot \rceil$ rounds a real number to its nearest integer. However, because of rounding, it is possible to obtain $\sum_{l=1}^{L} n_l \neq L\bar{n}$, which leads to $n \notin \mathcal{S}$. To solve this problem, we propose Algorithm 5.

In Algorithm 5, the elements of \boldsymbol{n} found in step 1 based on (17) are sorted in step 2 in decreasing order of $\{\alpha_1,\ldots,\alpha_L\}$, i.e., in increasing order of the sums of path loss $\{\beta_1,\ldots,\beta_L\}$, to generate $\{n_{[1]},\ldots,n_{[L]}\}$. Here, the order index [t] indicates that $n_{[t]}$ RF chains are chosen to be activated at the AP associated with the tth-smallest path loss. Therefore, if $\sum_{l=1}^L n_{[l]} < L\bar{n}$ and $n_{[t]} < N$, $n_{[t]}$ is increased by one. In contrast, if $\sum_{l=1}^L n_{[l]} > L\bar{n}$ and $n_{[L-t+1]} > 0$, $n_{[L-t+1]}$ is decreased by one. This process is repeated until $\boldsymbol{n} \in \mathcal{S}$ is satisfied, as shown in steps 3–13. In this procedure, by initializing t=1 and gradually increasing t, the numbers of turned-on RF chains for the APs with path loss are chosen to increase first, whereas those for the APs with larger path loss are chosen to decrease first. In step 14, $\{n_{[1]},\ldots,n_{[L]}\}$ are reordered into

Algorithm 5 Analog combining with PL-based SC-ARFA

```
Output: F^*
```

```
1: Find \mathbf{n} = \{n_1, \dots, n_L\} based on (17).
 2: Obtain \{n_{[1]}, \ldots, n_{[L]}\} s.t. \alpha_{[1]} > \ldots > \alpha_{[L]}.
 3: t = 1
 4: while n \notin S do
         if \sum_{l=1}^{L} n_{[l]} < L\bar{n} and n_{[t]} < N then
 6:
             n_{[t]} = n_{[t]} + 1
         end if
 7:
         if \sum_{l=1}^{L} n_{[l]} > L\bar{n} and n_{[L-t+1]} > 0 then
 8:
             n_{[L-t+1]} = n_{[L-t+1]} - 1
         end if
10:
11:
         t = t + 1
12:
         Reset t = 1 if t > L.
13: end while
14: Obtain \mathbf{n}^* by reordering \{n_{[1]}, \dots, n_{[L]}\} to the original order.
15: for l = 1 \to L do
         The CPU sends n_l^{\star} to the lth AP.
16:
         The lth AP determines its local analog combiner F_l^{\star} for n_l^{\star} RF chains, i.e., F_l^{\star} = [\tilde{f}_{l1}^{\star}, \dots, \tilde{f}_{ln_l^{\star}}^{\star}], where
17:
         \tilde{f}_{ln}^{\star} is given by (13).
```

18: **end for**

the original order. In steps 15–18, the numbers of active RF chains at the APs are determined, which are then fed back to the APs for SC-HBF, as in steps 3–6 of Algorithm 4.

D. Power consumption analysis

In this section, we analyze the power consumption of the proposed ARFA scheme compared to those of the non-adaptive RF chain activation, APS scheme in [11], and AS scheme in [28]. The power consumption is modeled based on [24], [43]–[45]. Specifically, each receive antenna needs a low-noise amplifier (LNA), a 90° hybrid and local oscillator (LO) buffer, and two mixers [43], [44], whereas each RF chain requires an ADC and N_r phase shifters, as illustrated in Fig. 1. Furthermore, an LO is shared by the entire operation at the AP [24], [43]–[45]. Therefore, the power consumed by the LO is required, even for an unactivated AP. Let P_{LO} , P_{LNA} , P_{PS} , P_{RF} , P_{ADC} , P_{M} , and P_{H} be the power consumed by an LO, LNA, phase shifter, RF chain, ADC, mixer, and 90° hybrid and LO buffer, respectively.

1) Fixed-activation HBF: We refer to the C- and SC-HBF without the ARFA as the fixed-activation HBF. In this scheme, the same number of RF chains are activated at all the L APs.

For comparison with the proposed ARFA schemes, we consider two deployments: $n_l = N, \forall l$ and $n_l = \bar{n}, \forall l$.

a) $n_l = N, \forall l$: In the fixed-activation HBF scheme with $n_l = N$, at each AP, power is consumed by N_r LNAs, N_r 90° hybrid and LO buffers, $2N_r$ mixers, NN_r phase shifters, N RF chains, N ADCs, and one LO. Therefore, the total power consumed by L APs is given by

$$\mathcal{P}_{\text{fixed}-N} = L \left[P_{\text{LO}} + N_r (P_{\text{LNA}} + 2P_{\text{M}} + P_{\text{H}}) + N N_r P_{\text{PS}} + N (P_{\text{RF}} + P_{\text{ADC}}) \right]$$

$$= L P_{\text{LO}} + L N (N_r P_{\text{PS}} + P_{\text{RF}} + P_{\text{ADC}}) + L N_r (P_{\text{LNA}} + 2P_{\text{M}} + P_{\text{H}}). \tag{18}$$

b) $n_l = \bar{n}, \forall l$: The total power consumption can be easily found by replacing N with \bar{n} in (18). As a result, the total power consumption in this scheme is given by

$$\mathcal{P}_{\text{fixed}-\bar{n}} = LP_{\text{LO}} + L\bar{n}(N_r P_{\text{PS}} + P_{\text{RF}} + P_{\text{ADC}}) + LN_r(P_{\text{LNA}} + 2P_{\text{M}} + P_{\text{H}}). \tag{19}$$

2) APS scheme: The APS scheme is proposed in [11] as an energy-efficient approach for sub-6-GHz band CF massive MIMO systems. In this scheme, only a subset of the APs is selected based on received power [11]. For comparison with the proposed schemes in mmWave systems, we assume the conventional deployment of RF chains at the APs, i.e., each AP is equipped with N RF chains, all of which are used for analog signal combining, i.e., $n_l = N, \forall l$. Therefore, each selected AP activates N RF chains for signal reception; hence, for a fair comparison, we assume that $\frac{L\bar{n}}{N}$ out of L APs with the largest received power are selected. This guarantees that a total of $L\bar{n}$ RF chains are used at the selected APs, which is equal to the number of activated RF chains in the proposed ARFA scheme and fixed-activation HBF scheme with $n_l = \bar{n}, \forall l$.

Note that the power consumption of P_{LO} is fixed for each AP. By replacing L in the second and last terms of (18) with $\frac{L\bar{n}}{N}$, the total power consumption in the APS scheme can be given as

$$\mathcal{P}_{APS} = LP_{LO} + L\bar{n}(N_r P_{PS} + P_{RF} + P_{ADC}) + \frac{L\bar{n}}{N} N_r (P_{LNA} + 2P_M + P_H). \tag{20}$$

3) AS scheme: In this work, we adopt the AS scheme for the CF mmWave massive MIMO system for comparison with our proposed schemes. Specifically, at each AP, only $N_r^{\rm AS}$ of N_r antennas are activated, corresponding to $N_r^{\rm AS}$ received signals put through the digital signal combining [28]. In other words, analog signal combining is conducted by a network of $N_r^{\rm AS}$ switches rather than NN_r phase shifters, in contrast to the other compared schemes. Therefore, at each AP, N_r switches are required, whereas the numbers of antennas, RF chains, ADCs, and 90° hybrid and LO buffers are the same and as small as $N_r^{\rm AS}$, and the number of mixers is $2N_r^{\rm AS}$.

Let P_{SW} be the power consumed by a switch. The total power consumption among all APs in this scheme is given as

$$\mathcal{P}_{AS} = LP_{LO} + LN_r P_{SW} + LN_r^{AS} (P_{RF} + P_{ADC} + P_{LNA} + 2P_M + P_H). \tag{21}$$

4) ARFA scheme: When the ARFA scheme is employed, at the lth AP, n_l RF chains, n_l ADCs, and $n_l N_r$ phase shifters are active and consume power. Additionally, the power is consumed by N_r LNAs, N_r 90° hybrid and LO buffers, and $2N_r$ mixers corresponding to N_r antennas. However, these components, except for the LO, are turned off if none of the RF chains are activated, i.e., $n_l = 0$, because all the RF chains are turned off in this case. As a result, the AP with $n_l = 0$ has a power consumption of only $P_{\rm LO}$, which is the same as that of an unselected AP in the APS scheme. Therefore, the power consumption of the lth AP can be expressed as

$$\mathcal{P}_{\text{ARFA}}^{(l)} = P_{\text{LO}} + n_l (N_r P_{\text{PS}} + P_{\text{RF}} + P_{\text{ADC}}) + \delta_{n_l} N_r (P_{\text{LNA}} + 2P_{\text{M}} + P_{\text{H}}),$$

where $\delta_{n_l} = 1$ if $n_l > 0$, and $\delta_{n_l} = 0$ if $n_l = 0$. Hence, the total power consumption of the ARFA scheme is given by

$$\mathcal{P}_{ARFA} = \sum_{l=1}^{L} \mathcal{P}_{ARFA}^{(l)} = LP_{LO} + L\bar{n}(N_r P_{PS} + P_{RF} + P_{ADC}) + N_r (P_{LNA} + 2P_M + P_H) \sum_{l=1}^{L} \delta_{n_l},$$
(22)

where the last equality is obtained by $\sum_{l=1}^{L} n_l = L\bar{n}$, as explained in Section IV-A. We note that the proposed TS-aided C-ARFA, FS-aided C-ARFA, and SC-ARFA algorithms have different operations, which can result in different values of $\sum_{l=1}^{L} \delta_{n_l}$ in (22). Therefore, the proposed ARFA schemes can have different power consumption, even though the total number of turned-on RF chains at APs are the same.

By comparing (22) to (18)–(20), we observe that:

- The proposed ARFA scheme requires no higher power consumption than the fixed-activation HBF schemes with $n_l = N$ and $n_l = \bar{n}, \forall l$, because $\bar{n} < N$ and $\sum_{l=1}^L \delta_{n_l} \leq L$.
- Both the power consumption and total achievable rate of the proposed ARFA scheme significantly depend on \bar{n} . Specifically, a smaller \bar{n} leads to a reduction in both power consumption and total achievable rate with respect to the fixed-activation HBF scheme with $n_l = N, \forall l$. This tradeoff is discussed further in the next section.
- It is observed from (20) and (22) that the APS and proposed ARFA schemes have a difference of $\left|\frac{L\bar{n}}{N} \sum_{l=1}^{L} \delta_{n_l}\right| N_r (P_{\text{LNA}} + 2P_{\text{M}} + P_{\text{H}})$ in power consumption, even though

Table I. Simulation parameters of the path-loss model [39]

Parameters	Values	
Frequency	$f_c = 28 \; \mathrm{GHz}$	
Bandwidth	B = 100 MHz	
Noise figure	NF = 9 dB	
Antenna gains	$G_{\mathrm{TX}} = 15 \; \mathrm{dBi}, \; G_{\mathrm{RX}} = 24.5 \; \mathrm{dBi}$	
Path-loss exponents	$\epsilon_{\text{LOS}} = 1.9, \epsilon_{\text{NLOS}} = 4.1$	
Standard deviation of shadowing factor	$\xi_{\text{LOS}} = 1.1, \xi_{\text{NLOS}} = 7.6$	
Outage/LOS parameters	$1/a_{\text{out}} = 45.5 \text{ m}, b_{\text{out}} = 3.3, 1/a_{\text{LOS}} = 37 \text{ m}$	

they have the same total number of active RF chains. Specifically, the APS scheme requires slightly lower power consumption, but its achievable rate is much lower than that of the ARFA scheme, as is shown in the next section. It is not certain from (21) and (22) which of AS and ARFA schemes has the lower power consumption, which will be determined based on the simulation results in the next section.

V. SIMULATION RESULTS

A. Simulation parameters

Simulations are performed to evaluate the total achievable rates, power consumption, EEs, and computational complexities of the proposed C-HBF, SC-HBF, and ARFA schemes. In simulations, K UEs and L APs are uniformly distributed at random within a square coverage area of size $D \times D$ m², where D is set to 200 m [5]. The parameters of the path-loss model, presented in Table I, are assumed based on the directional close-in reference distance path-loss model for the 28-GHz mmWave system in [39]. They are used to compute the probabilities of outage, line-of-sight (LOS), and non-LOS (NLOS) as $p_{\text{out}}(d) = \max\left\{0, 1 - e^{-a_{\text{out}}d + b_{\text{out}}}\right\}$, $p_{\text{LOS}}(d) = [1 - p_{\text{out}}(d)] e^{-a_{\text{LOS}}d}$, and $p_{\text{NLOS}}(d) = 1 - p_{\text{out}}(d) - p_{\text{LOS}}(d)$, respectively [5]. Then, the large-scale fading coefficients are computed based on (5). Furthermore, the total antenna gain and noise power are given as $G_a = G_{\text{TX}} + G_{\text{RX}}$ and $N_0 = -174 \text{ dBm/Hz} + 10 \log_{10}(B) + \text{NF}$, respectively.

The channel coefficients between each UE and AP are generated based on the geometric Saleh–Valenzuela channel model given in (4). For simplicity, we assume an identical number of effective channel paths between each UE and AP, which is set to $P_{kl}=3, \forall l, k$ [1], [33], [46], reflecting the limited scattering in mmWave channels. The AoDs and AoAs are uniformly distributed in $\left[-\frac{\pi}{6}, \frac{\pi}{6}\right]$ and $\left[-\frac{\pi}{12}, \frac{\pi}{12}\right]$, respectively. The ULA model is employed for the antenna arrays at the APs and UEs with antenna spacing of half a wavelength, i.e., $\frac{d_s}{\lambda}=\frac{1}{2}$ [42], [47]. The phases in the analog combiner are selected from $\Theta=\left\{0,\frac{2\pi}{2^b},\frac{4\pi}{2^b},\ldots,\frac{2(2^b-1)\pi}{2^b}\right\}$, where b=4 is set, implying 4-bit quantization of the phase shifters.

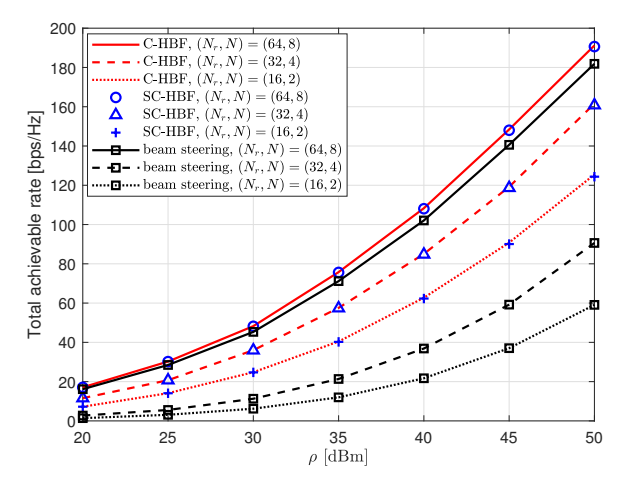


Fig. 2. Total achievable rates of the C-HBF and SC-HBF schemes compared to those of the beam steering scheme with $L=40, K=8, N_t=4, (N_r,N)=\{(16,2), (32,4), (64,8)\}.$

B. Performance of the C-HBF and SC-HBF schemes

We numerically evaluate the total achievable rates of the C-HBF and SC-HBF schemes, which are analyzed in Section III. We assume the conventional RF chain deployment in this section, i.e., all the N available RF chains are active for analog combining. For comparison, we consider the beam steering scheme, in which the phase shifters are used to optimally orient the array response in space [21], [32]. In other words, the phases of the analog combining coefficients are obtained by quantizing those of the array response vectors that match best with the dominant eigenmode of the channel matrix.

Fig. 2 shows the total achievable rates of the C-HBF, SC-HBF, and beam steering schemes with $N_t = 4$, L = 40, and K = 8 [21]. At the APs, the number of RF chains N is set depending on N_r as follows: $(N_r, N) = \{(16, 2), (32, 4), (64, 8)\}$. It is clearly seen in Fig. 2 that in all the considered systems, the SC-HBF scheme approximately achieves the total achievable rate of the C-HBF scheme, as stated in Theorem 2. The C-HBF scheme performs slightly better than the SC-HBF scheme for $(N_r, N) = (16, 2)$ at high ρ . However, for the larger systems, i.e., $(N_r, N) = \{(32, 4), (64, 8)\}$, they perform very close to each other. It is also observed in Fig. 2 that the proposed C-HBF and SC-HBF schemes outperform the beam steering approach since beam steering alone cannot perfectly capture the channel's dominant eigenmodes [32].

C. Performance of the proposed ARFA scheme

The total achievable rates, power consumption, and EEs of the proposed ARFA schemes, namely, TS-aided C-ARFA, FS-aided C-ARFA, PL-based SC-ARFA, and SV-based SC-ARFA, are compared to those of the fixed-activation HBF with $n_l = N$ and $n_l = \bar{n}, \forall l$, APS, and AS schemes discussed in Section IV-D. In our simulations, C-HBF is used for the fixed-activation HBF and APS schemes. We note that the C- and SC-HBF provides almost identical

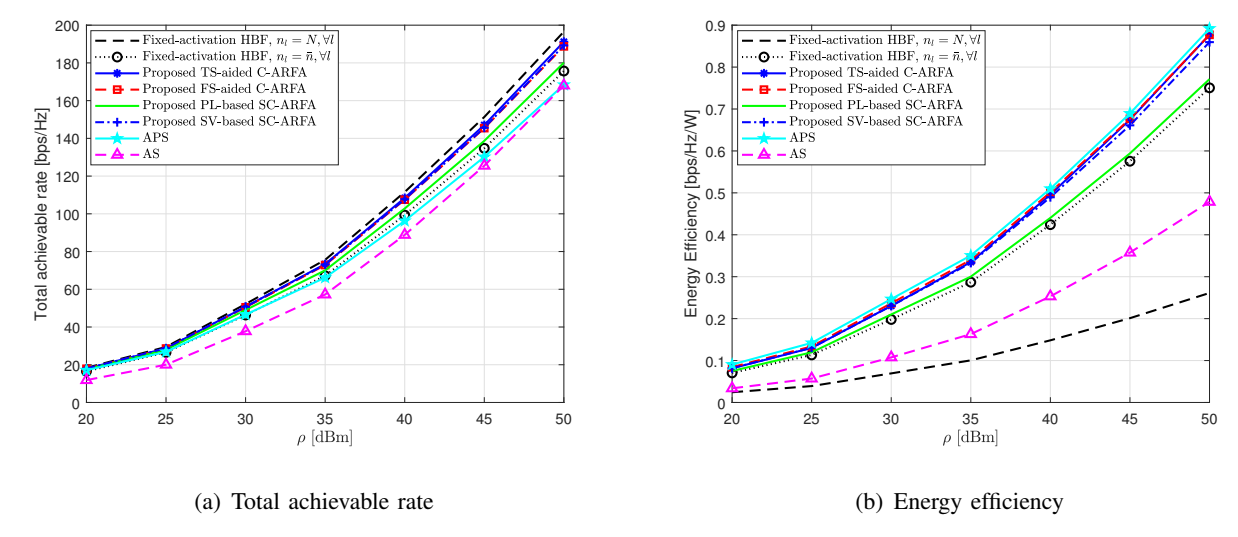


Fig. 3. Total achievable rates and EEs of the proposed ARFA schemes compared to those of the fixed-activation HBF with $n_l = N$, $n_l = \bar{n}, \forall l$, APS, and AS schemes. Simulation parameters are $L = 40, K = 8, N_t = 4, N_r = 64, N = 8$, and $\bar{n} = 2$. performance, as shown in Fig. 2, and for the same RF chain deployment, they have the same power consumption. We consider a CF mmWave massive MIMO system with $L=40~\mathrm{APs}$ and K=8 UEs [21], whereas $(N_r,N)=(64,8)$ [5] and $\bar{n}=2$ are assumed at each AP. In the TS-aided C-ARFA scheme, the number of search iterations should be proportional to L and sufficiently large to guarantee the near-optimal performance. Therefore, we set $\mathcal{I}=8L$ and $count_{max} = \mathcal{I}/2$. In the AS scheme, the number of selected antennas at each AP is set to $N_r^{\rm AS}=32$, which ensures that the AS scheme achieves comparable total achievable rates with respect to the proposed schemes, allowing us to compare them in terms of EE. In the simulations, the power consumption of the fixed-activation HBF schemes with $n_l = N$, $n_l = \bar{n}$, the APS, and AS scheme is computed based on (18)–(21), whereas that of the proposed ARFA schemes is obtained through simulations because it depends on δ_{n_i} , as indicated in (22). To compute the power consumption in (18)–(22), we use the same assumptions as in [24], [43]–[45], i.e., $P_{\mathrm{LNA}} = 20 \,\,\mathrm{mW}, \, P_{\mathrm{ADC}} = 200 \,\,\mathrm{mW}, \, P_{\mathrm{RF}} = 40 \,\,\mathrm{mW}, \, P_{\mathrm{PS}} = 30 \,\,\mathrm{mW}, \, P_{\mathrm{M}} = 0.3 \,\,\mathrm{mW}, \, P_{\mathrm{H}} = 3 \,\,\mathrm{mW}, \, P_{\mathrm{H}} = 10.0 \,\,\mathrm{mW}$ $P_{\text{SW}} = 5 \text{ mW}$, and $P_{\text{LO}} = 22.5 \text{ mW}$. Then, the EE of a scheme is calculated as the ratio between the total achievable rate and the total power consumption [11].

In Fig. 3, we show the total achievable rates and EEs of the considered schemes versus the average transmit power ρ . From Fig. 3, the following observations are noted:

• The fixed-activation HBF scheme with $n_l = N$ achieves the highest total achievable rate, as seen in Fig. 3(a), because it activates all the available APs and RF chains. However, in this scheme, high power is consumed by LN RF chains. Therefore, its EE is significantly lower than those of the other considered schemes, in which only $L\bar{n}$ ($\ll LN$) RF chains

are turned on, as seen in Fig. 3(b).

• The proposed TS-aided C-ARFA, FS-aided C-ARFA, and SV-based SC-ARFA perform similarly and achieve remarkable improvement in EE with marginal loss in total achievable rate with respect to the fixed-activation HBF scheme with $n_l = N$. Specifically, at $\rho = 50$ dBm, they have the performance loss of approximately 2.7–3.7%, whereas approximately 230–236% improvement in EE is attained compared to that obtained using the fixed-activation HBF scheme with $n_l = N$. However, those for the PL-based SC-ARFA show an 8.4% loss in total rate and 195.3% improvement in EE. However, the PL-based SC-ARFA scheme still outperforms the APS, AS, and fixed-activation HBF schemes with $n_l = \bar{n}$. Furthermore, because it is based only on the large-scale fading channels, it attains a significant reduction in fronthauling load, as demonstrated in Section V-E. It is also observed that the proposed ARFA schemes outperform the APS and AS schemes in terms of the total achievable rate. The fixed-activation HBF scheme with $n_l = \bar{n}$ is outperformed by the proposed ARFA schemes in both achievable rate and EE. It is also clear that the AS scheme is not an energy-efficient scheme for the CF mmWave massive MIMO system.

In Fig. 4, we show the total achievable rates and EEs of the considered schemes versus the number of APs. In this figure, we use the same simulation parameters as in Fig. 3, except for the varying numbers of APs, i.e., $L = \{20, 40, 60, 80\}$, and $\rho = 50$ dBm. In Fig. 4, the observations on the achievable rates and EEs of the considered schemes are similar to those from Fig. 3. In particular, it is seen that in the entire range of L, the proposed TS-aided C-ARFA, FS-aided C-ARFA, SV-aided ARFA schemes have marginal losses in total achievable rate with respect to the fixed-activation HBF scheme with $n_l = N$. The total achievable rate of the PL-based SC-ARFA scheme approaches those of the other proposed ARFA schemes, as L increases. Furthermore, the proposed ARFA schemes outperform the APS scheme in terms of EEs for a moderate number of APs, i.e., L = 20, whereas for $L \geq 40$, they perform comparably. In particular, as L increases, the AS scheme becomes less spectral efficient, whereas for all the considered values of L, its EE is far worse than that of the proposed schemes and only better than the fixed-activation HBF scheme with $n_l = \bar{n}$.

To summarize, we can conclude from Figs. 3 and 4 that when a limited number of RF chains are used, equally activating the same number of RF chains at the APs, as in the fixed-activation HBF scheme with $n_l = N$ or $n_l = \bar{n}$, is relatively energy-inefficient. Furthermore, although the APS scheme is energy-efficient approach, it has significant losses in total achievable rate.

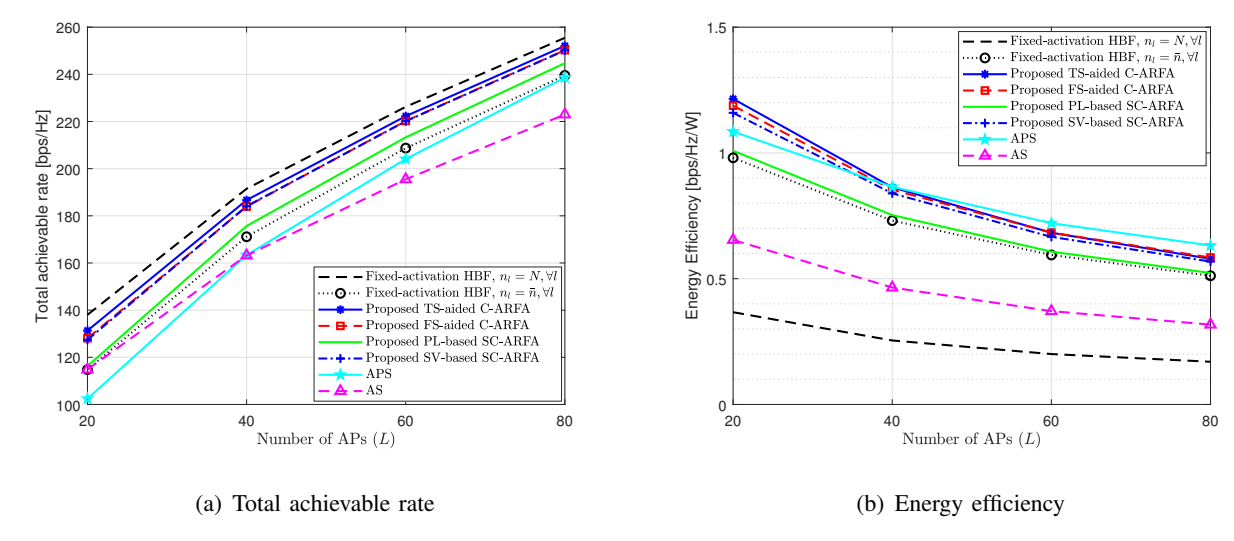


Fig. 4. Total achievable rates and EEs of the proposed ARFA schemes compared to those of the fixed-activation HBF with $n_l=N,\ n_l=\bar{n}, \forall l,$ APS, and AS schemes. Simulation parameters are $L=\{20,40,60,80\},\ K=8,\ N_t=4,\ N_r=64,\ N=8,\ \bar{n}=2,$ and $\rho=50$ dBm.

In contrast, the proposed ARFA schemes achieve the highest or nearly highest performance in terms of both spectral and energy efficiency, which are both far better than those of the AS scheme.

D. Tradeoff between achievable rates and power consumption

The total achievable rate and power consumption of the considered schemes versus \bar{n} are evaluated numerically in Fig. 5 for $L=40, K=8, N_r=64, N_t=4, N=8, \bar{n}=\{1,2,\ldots,8\},$ and $\rho=50$ dBm. From Fig. 5, the following observations can be noted:

- The total achievable rate and power consumption of the fixed-activation HBF with $n_l=N$ and those of the AS scheme remain unchanged with \bar{n} because N and $N_r^{\rm AS}$ RF chains, respectively, are always active at every AP. In contrast, those of the other schemes depend on \bar{n} . Specifically, as \bar{n} increases, both the total achievable rate and power consumption of the fixed-activation HBF scheme with $n_l=\bar{n}$, proposed ARFA, and APS schemes increase to approach those of the fixed-activation HBF with $n_l=N$.
- In Fig. 5(a), the proposed ARFA schemes perform closest to the fixed-activation HBF scheme with $n_l=N$, even for a small \bar{n} . In terms of power consumption, they require slightly higher power than the APS scheme. However, their EEs are comparable, as seen in Figs. 3 and 4, owing to the efficient use of RF chains. Furthermore, for $\bar{n} \geq 4$, the AS scheme has the lowest power consumption at the cost of the smallest total achievable rate.
- For the optimal performance-power consumption tradeoff in the assumed environment, $\bar{n}=2$ can be chosen in the proposed TS- and FS-aided C-ARFA and SV-based SC-ARFA schemes to achieve 70.7–71.5% power reduction with only approximately 2.7–3.7%

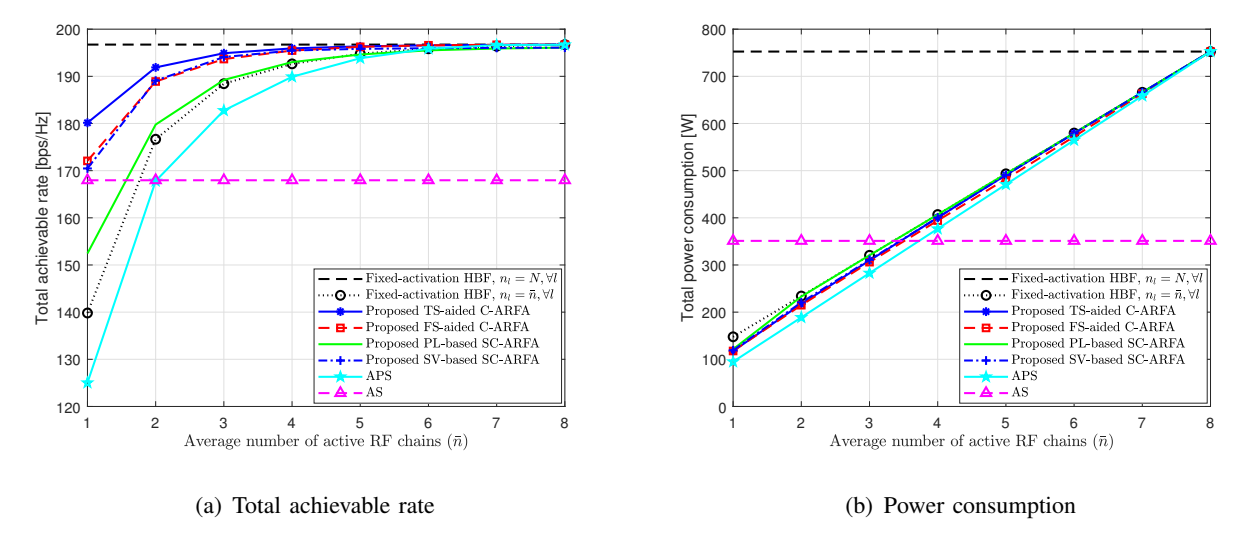


Fig. 5. Total achievable rates and EEs of the proposed ARFA schemes compared to those of the fixed-activation HBF with $n_l=N,\ n_l=\bar{n}, \forall l,$ and APS schemes. Simulation parameters are $L=40,\ K=8,\ N_t=4,\ N_r=64,\ N=8,$ $\bar{n}=\{1,2,\ldots,8\},$ and $\rho=50$ dBm.

Table II. Average amounts of information exchange between the CPU and an AP on the fronthaul links in the proposed C-HBF, SC-HBF, C-ARFA, and SC-ARFA schemes

Schemes	AP to CPU	CPU to AP
C-HBF	$N_r K N_t$ complex numbers	N_rN real numbers
TS- and FS-aided C-ARFA	$N_r K N_t$ complex numbers	$N_r \bar{n}$ real numbers
SC-HBF	NKN_t complex numbers	0
SV-based SC-ARFA	$\bar{n}KN_t$ complex numbers and N real numbers	1 real number
PL-based SC-ARFA	$\bar{n}KN_t$ complex numbers	1 real number

performance loss. With $\bar{n}=1$, only a single RF chain on average is turned on at each AP, resulting in performance losses of 8.4%, 12.5%, 13.3%, 22.5%, 36.5%, 28.9%, and 14.6% in the TS-, FS-aided C-ARFA, SV-, PL-based SC-ARFA, APS, fixed-activation HBF with $n_l=\bar{n}$, and AS schemes, respectively, compared to the case of $n_l=N$.

E. Fronthauling load and computational complexity

In this section, we evaluate the amount of information exchange between the CPU and APs and the computational load, which are presented in Tables II and III, respectively.

1) Fronthauling loads: In the C-HBF scheme, the CSI for H_l of size $N_r \times KN_t$ is sent from the lth AP to the CPU, which is used at the CPU to generate F_l of size $N_r \times N$. However, we note that all the entries of F_l have constant amplitudes of $\frac{1}{\sqrt{N_r}}$. Therefore, only N_rN real numbers representing the phases are fed back on the reverse link. A similar analysis is valid for the TS- and FS-aided C-ARFA schemes with the note that only an average of $N_r\bar{n}$ real numbers need to be fed back from the APs to the CPU because in these schemes, only an average of \bar{n} RF chains are activated. It is observed that the amount of information exchange between the CPU and APs is relatively large in the C-HBF and C-ARFA schemes.

Table III. Computational complexities of the TS- and FS-aided C-ARFA schemes with $L=\{20,40,60,80\},~K=8,$ $N_t=4,~N_r=64,~N=8,~\bar{n}=2,$ and $\rho=50$ dBm.

Number of APs	TS-aided C-ARFA	FS-aided C-ARFA	Complexity reduction
L = 20	260	43	83.5%
L = 40	1250	89	92.9%
L = 60	3002	135	95.5%
L = 80	5711	179	96.9%

In contrast, those for the SC-HBF and SC-ARFA schemes are small. Specifically, in the SC-HBF scheme, NKN_t complex numbers representing an analog-combined channel matrix are sent from each AP to the CPU for signal decoding. In contrast, those for the SV- and PL-based SC-ARFA schemes are as small as $\bar{n}KN_t$ on average due to the reduced number of active RF chains. Additionally, in the SV-based SC-ARFA scheme, N real numbers for the N singular values are sent from an AP to the CPU for each channel variation, whereas the transmission of path loss values in the PL-based SC-ARFA scheme can be ignored because of their slow variations. On the reverse link from the CPU to an AP, only a single real number, which is the number of active RF chains, is fed back in the SV- and PL-based SC-ARFA schemes, as demonstrated in Algorithms 4 and 5, respectively. Given that $N \ll N_r$, the SC-based schemes require much less information exchange between the CPU and each AP compared to the C-HBF and C-ARFA schemes. Furthermore, with the note that $\bar{n} \ll N$, ARFA can significantly reduce the fronthauling loads for SC-HBF.

2) Computational loads: The SC-HBF scheme is definitely computationally cheaper than the C-HBF scheme, as analyzed in Section III-B. Therefore, we focus on comparing the computational complexities of the proposed ARFA schemes. It is observed from Algorithms 2 and 3 that the overall complexities of the TS- and FS-aided C-ARFA schemes are approximately proportional to the number of examined candidates, i.e., n. In contrast, candidate examination is not performed in the SC-ARFA scheme. Therefore, in this section, the complexities of the TS- and FS-aided C-ARFA schemes are evaluated based on the number of candidates examined in Algorithms 2 and 3, respectively, whereas that of the SC-ARFA scheme is omitted. Furthermore, to ensure that the complexities of the TS- and FS-aided C-ARFA are compared for approximately the same performance, the simulation parameters are assumed to be the same as those in Fig. 4. It is seen from Table III and Fig. 4 that the FS-aided C-ARFA scheme requires significantly lower complexity than that required by the TS-aided C-ARFA scheme to achieve almost the same performance. Specifically, the complexity-reduction ratios are higher than 90% for $L = \{40, 60, 80\}$. Furthermore, the larger L is, the more significant complexity reduction is

attained by the FS-aided C-ARFA scheme with respect to the TS-aided C-ARFA scheme.

VI. CONCLUSION

In this work, we propose two HBF schemes for CF mmWave massive MIMO systems, including C-HBF and SC-HBF, in which the analog combiners are generated at the CPU based on the global CSI and at each AP based on the local CSI, respectively. Notably, although the SC-HBF requires substantially lower computational complexity and no information exchange between the CPU and APs, it achieves approximately the same total achievable rate as that obtained by the C-HBF scheme. Furthermore, to reduce the power consumption in the CF mmWave massive MIMO system, we propose adaptive activation of RF chains at the APs. Three algorithms are developed to select the number of active RF chains at the APs such that the system's power consumption is significantly reduced with only a marginal loss in total achievable rate. The efficiency of the proposed schemes is justified by the simulation results, which show that the proposed ARFA scheme achieves up to 245% improvement in EE while leading to a loss of only approximately 2.5% in total achievable rate. In the proposed HBF and ARFA schemes, perfect CSI is assumed for the design of the beamformers. However, in general CF mmWave massive MIMO systems, it is impractical to obtain perfect CSI, owing to the requirement of excessive training overhead as well as the channel estimation error and pilot contamination. Therefore, the optimization and analysis of HBF schemes for CF mmWave massive MIMO systems with the imperfect CSI would be an interesting research topic for future work. Furthermore, the capacity-achieving advanced digital receiver is assumed to facilitate the analysis and optimization of the analog part in the proposed schemes. However, in practical systems, low-complexity digital receivers can instead be considered to reduce the complexity; thus, the optimization of the proposed schemes incorporated with low-complexity digital receiver can be considered for future work. Moreover, further optimization of the proposed analog combining schemes to specialize wideband systems is also considered for future research.

APPENDIX A

PROOF OF THEOREM 1

Because F is a block-diagonal matrix, we have $H^HF = [H_1^HF_1, H_2^HF_2, \dots, H_L^HF_L]$, leading to $H^HFF^HH = \sum_{l=1}^L H_l^HF_lF_l^HH_l$. Therefore, Q in (6) can be expressed as $Q = I_{KN_t} + I_{KN_t}$

 $\gamma \sum_{l=1}^{L} \boldsymbol{H}_{l}^{H} \boldsymbol{F}_{l} \boldsymbol{F}_{l}^{H} \boldsymbol{H}_{l}$. By letting $\boldsymbol{G}_{l} = \boldsymbol{H}_{l}^{H} \boldsymbol{F}_{l} \boldsymbol{F}_{l}^{H} \boldsymbol{H}_{l}$, \boldsymbol{Q} can be further expanded as

$$Q = \underbrace{I_{KN_t} + \gamma G_1}_{\triangleq E_1} + \gamma G_2 + \dots + \gamma G_L = E_1 \underbrace{(I_{KN_t} + \gamma E_1^{-1} G_2}_{\triangleq E_2} + \dots + \gamma E_1^{-1} G_L)$$

$$= E_1 E_2 \underbrace{(I_{KN_t} + \gamma E_2^{-1} E_1^{-1} G_2}_{\triangleq E_2} + \dots + \gamma E_2^{-1} E_1^{-1} G_L) = \dots = E_1 E_2 \dots E_L,$$
(23)

where $E_l = I_{KN_t} + \gamma (E_1 \dots E_{l-1})^{-1} G_l$, $l = 2, 3, \dots, L$. As a result, the total achievable rate can be expressed as

$$R = \log_2 \det \mathbf{Q} = \sum_{l=1}^{L} \log_2 \det(\mathbf{E}_l) = \sum_{l=1}^{L} \log_2 \det(\mathbf{I}_{KN_t} + \gamma (\underbrace{\mathbf{E}_1 \dots \mathbf{E}_{l-1}})^{-1} \mathbf{G}_l)$$
(24)

$$= \sum_{l=1}^{L} \log_2 \det \left(\mathbf{I}_{KN_t} + \gamma \mathbf{Q}_{l-1}^{-1} \mathbf{H}_l^H \mathbf{F}_l \mathbf{F}_l^H \mathbf{H}_l \right) = \sum_{l=1}^{L} \log_2 \det \left(\mathbf{I}_N + \gamma \mathbf{F}_l^H \mathbf{H}_l \mathbf{Q}_{l-1}^{-1} \mathbf{H}_l^H \mathbf{F}_l \right), \quad (25)$$

as given in (7) in Theorem 1. The last equality in (25) follows from $\det(\boldsymbol{I}_{KN_t} + \boldsymbol{A}\boldsymbol{B}) = \det(\boldsymbol{I}_N + \boldsymbol{B}\boldsymbol{A})$ with $\boldsymbol{A} = \boldsymbol{Q}_{l-1}^{-1}\boldsymbol{H}_l^H\boldsymbol{F}_l \in \mathbb{C}^{KN_t \times N}$ and $\boldsymbol{B} = \boldsymbol{F}_l^H\boldsymbol{H}_l \in \mathbb{C}^{N \times KN_t}$. Furthermore, from the definition of \boldsymbol{Q}_{l-1} in (24), we have $\boldsymbol{E}_{l-1} = \boldsymbol{I}_{KN_t} + \gamma(\boldsymbol{E}_1 \dots \boldsymbol{E}_{l-2})^{-1}\boldsymbol{G}_{l-1} = \boldsymbol{I}_{KN_t} + \gamma\boldsymbol{Q}_{l-2}^{-1}\boldsymbol{G}_l$. Finally, recalling that $\boldsymbol{G}_l = \boldsymbol{H}_l^H\boldsymbol{F}_l\boldsymbol{F}_l^H\boldsymbol{H}_l$, we obtain the expression of \boldsymbol{Q}_{l-1} in (9), i.e.,

$$Q_{l-1} = Q_{l-2}E_{l-1} = Q_{l-2}(I_{KN_t} + \gamma Q_{l-2}^{-1}G_l) = Q_{l-2} + \gamma H_{l-1}^H F_{l-1}F_{l-1}^H H_{l-1},$$
(26)

with $\boldsymbol{Q}_0 = \boldsymbol{I}_{KN_t}$, which completes the proof.

APPENDIX B

PROOF OF THEOREM 2

From (26), Q_{l-1} in (8) can be expressed as

$$\mathbf{Q}_{l-1} = \mathbf{I}_{KN_t} + \gamma \sum_{i=1}^{l-1} \mathbf{H}_i^H \mathbf{F}_i \mathbf{F}_i^H \mathbf{H}_i, l = 2, \dots, L.$$

$$(27)$$

1) When l is small: With the assumption of very low SNRs in CF mmWave massive MIMO, we have $\mathbf{Q}_{l-1} \approx \mathbf{I}_{KN_t}$ for small l, leading to

$$R_l \approx \tilde{R}_l = \log_2 \det \left(\mathbf{I}_N + \gamma \mathbf{F}_l^H \mathbf{H}_l \mathbf{H}_l^H \mathbf{F}_l \right), \tag{28}$$

where R_l is the sub-rate associated with the lth AP in C-HBF, given in (8). The unconstrained combiner that maximizes \tilde{R}_l in (28) is the matrix with columns being the N singular vectors corresponding to the N largest singular values of H_l . As a result, the analog combining vectors in the SC-HBF scheme can be determined as in (13).

2) As l increases: Because F_i only depends on H_i for small l, $\{H_i^H F_i F_i^H H_i\}$, $i = 1, \ldots, l-1$ are independent of each other. As l grows and becomes sufficiently large, by the law of large numbers, we have $\sum_{i=1}^{l-1} H_i^H F_i F_i^H H_i \rightarrow (l-1)\bar{E}$, where $\bar{E} = \mathbb{E} \{H_i^H F_i F_i^H H_i\}$ has constant diagonal elements and zeros for off-diagonal elements. Therefore, Q_{l-1} in (27) becomes approximately diagonal even when l is large, as does Q_{l-1}^{-1} .

Based on the ordered singular value decomposition, \mathbf{H}_l can be factorized as $\mathbf{H}_l = \mathbf{U} \mathbf{\Sigma} \mathbf{V}^H$, where $\mathbf{\Sigma}$ is an $N_r \times K N_t$ rectangular diagonal matrix with the singular values of \mathbf{H}_l on the main diagonal in decreasing order, whereas \mathbf{U} and \mathbf{V} are unitary matrices of size $N_r \times N_r$ and $K N_t \times K N_t$, whose columns are the left- and right-singular vectors of \mathbf{H}_l , respectively. Then, R_l in (8) can be expressed as

$$R_{l} = \log_{2} \det(\boldsymbol{I}_{N} + \gamma \boldsymbol{F}_{l}^{H} \boldsymbol{U} \underbrace{\boldsymbol{\Sigma} \boldsymbol{V}^{H} \boldsymbol{Q}_{l-1}^{-1} \boldsymbol{V} \boldsymbol{\Sigma}^{H}}_{\triangleq \boldsymbol{\Lambda}} \boldsymbol{U}^{H} \boldsymbol{F}_{l}).$$
(29)

Because Q_{l-1}^{-1} is approximately a diagonal matrix with constant diagonal elements, as shown above, $\Lambda = \Sigma V^H Q_{l-1}^{-1} V \Sigma^H$ becomes approximately a diagonal matrix, and its diagonal elements are in decreasing order. Therefore, the optimal solution of $\max_{F_l} R_l = \log_2 \det(I_N + \gamma F_l^H U \Lambda U^H F_l)$ is approximately the matrix with columns being the first N columns of U, which are the singular vectors corresponding to the N largest singular values of H_l , implying the analog combining vectors given in (13) for SC-BF. This completes the proof.

REFERENCES

- [1] N. T. Nguyen and K. Lee, "Coverage and Cell-Edge Sum-Rate Analysis of mmWave Massive MIMO Systems With ORP Schemes and MMSE Receivers," *IEEE Trans. Signal Process.*, vol. 66, no. 20, pp. 5349–5363, 2018.
- [2] M. R. Akdeniz, Y. Liu, M. K. Samimi, S. Sun, S. Rangan, T. S. Rappaport, and E. Erkip, "Millimeter wave channel modeling and cellular capacity evaluation," *IEEE J. Sel. Areas Commun.*, vol. 32, no. 6, pp. 1164–1179, 2014.
- [3] H. Q. Ngo, A. Ashikhmin, H. Yang, E. G. Larsson, and T. L. Marzetta, "Cell-free massive MIMO: Uniformly great service for everyone," in *IEEE 16th Int. Workshop Signal Process. Advances in Wireless Commun. (SPAWC)*, 2015, pp. 201–205.
- [4] —, "Cell-free massive MIMO versus small cells," IEEE Trans. Wireless Commun., vol. 16, no. 3, pp. 1834–1850, 2017.
- [5] G. Femenias and F. Riera-Palou, "Cell-Free Millimeter-Wave Massive MIMO Systems With Limited Fronthaul Capacity," IEEE Access, vol. 7, pp. 44596–44612, 2019.
- [6] G. Interdonato, H. Q. Ngo, P. Frenger, and E. G. Larsson, "Downlink training in cell-free massive MIMO: A blessing in disguise," *IEEE Trans. Wireless Commun.*, vol. 18, no. 11, pp. 5153–5169, 2019.
- [7] A. Papazafeiropoulos, P. Kourtessis, M. Di Renzo, S. Chatzinotas, and J. M. Senior, "Performance Analysis of Cell-Free Massive MIMO Systems: A Stochastic Geometry Approach," *IEEE Trans. Veh. Tech.*, vol. 69, no. 4, pp. 3523–3537, 2020.
- [8] E. Nayebi, A. Ashikhmin, T. L. Marzetta, and H. Yang, "Cell-free massive MIMO systems," in *IEEE Asilomar Conf. Signals, Systems and Computers*, 2015, pp. 695–699.

- [9] E. Björnson and L. Sanguinetti, "Making cell-free massive MIMO competitive with MMSE processing and centralized implementation," *IEEE Trans. Wireless Commun.*, 2019.
- [10] L. D. Nguyen, T. Q. Duong, H. Q. Ngo, and K. Tourki, "Energy efficiency in cell-free massive MIMO with zero-forcing precoding design," *IEEE Commun. Lett.*, vol. 21, no. 8, pp. 1871–1874, 2017.
- [11] H. Q. Ngo, L.-N. Tran, T. Q. Duong, M. Matthaiou, and E. G. Larsson, "On the total energy efficiency of cell-free massive MIMO," *IEEE Trans. Green Commun. and Network.*, vol. 2, no. 1, pp. 25–39, 2017.
- [12] M. Bashar, K. Cumanan, A. G. Burr, H. Q. Ngo, E. G. Larsson, and P. Xiao, "Energy efficiency of the cell-free massive MIMO uplink with optimal uniform quantization," *IEEE Trans. Green Commun. Networking*, vol. 3, no. 4, pp. 971–987, 2019.
- [13] G. Interdonato, P. Frenger, and E. G. Larsson, "Scalability aspects of cell-free massive MIMO," in *IEEE Int. Conf. Commun.* (*ICC*), 2019, pp. 1–6.
- [14] E. Björnson and L. Sanguinetti, "Scalable cell-free massive MIMO systems," IEEE Trans. Commun., 2020.
- [15] S. E. Hajri, J. Denis, and M. Assaad, "Enhancing Favorable Propagation in Cell-Free Massive MIMO Through Spatial User Grouping," in *IEEE Int. Workshop Signal Process. Advances Wireless Commun. (SPAWC)*, 2018, pp. 1–5.
- [16] X. Hu, C. Zhong, X. Chen, W. Xu, H. Lin, and Z. Zhang, "Cell-free massive MIMO systems with low resolution ADCs," *IEEE Trans. Commun.*, vol. 67, no. 10, pp. 6844–6857, 2019.
- [17] E. Nayebi, A. Ashikhmin, T. L. Marzetta, H. Yang, and B. D. Rao, "Precoding and power optimization in cell-free massive MIMO systems," *IEEE Trans. Wireless Commun.*, vol. 16, no. 7, pp. 4445–4459, 2017.
- [18] J. Zhang, Y. Wei, E. Björnson, Y. Han, and S. Jin, "Performance analysis and power control of cell-free massive MIMO systems with hardware impairments," *IEEE Access*, vol. 6, pp. 55302–55314, 2018.
- [19] S. Buzzi and C. D'Andrea, "Cell-free massive MIMO: User-centric approach," *IEEE Wireless Commun. Lett.*, vol. 6, no. 6, pp. 706–709, 2017.
- [20] S.-H. Park, O. Simeone, Y. C. Eldar, and E. Erkip, "Optimizing Pilots and Analog Processing for Channel Estimation in Cell-Free Massive MIMO with One-Bit ADCs," in *IEEE Int. Workshop Signal Process. Advances Wireless Commun.* (SPAWC), 2018, pp. 1–5.
- [21] J. Li, D.-W. Yue, and Y. Sun, "Performance analysis of millimeter wave massive MIMO systems in centralized and distributed schemes," *IEEE Access*, vol. 6, pp. 75482–75494, 2018.
- [22] M. Alonzo and S. Buzzi, "Cell-free and user-centric massive MIMO at millimeter wave frequencies," in *IEEE Annual Int. Symposium Personal, Indoor, and Mobile Radio Communications (PIMRC)*, 2017, pp. 1–5.
- [23] M. Alonzo, S. Buzzi, A. Zappone, and C. D'Elia, "Energy-Efficient Power Control in Cell-Free and User-Centric Massive MIMO at Millimeter Wave," *IEEE Trans. Green Commun. Network.*, 2019.
- [24] N. T. Nguyen and K. Lee, "Unequally Sub-connected Architecture for Hybrid Beamforming in Massive MIMO Systems," *IEEE Trans. Wireless Commun.*, vol. 19, no. 2, pp. 1127–1140, Feb. 2020.
- [25] H. Liu, J. Zhang, X. Zhang, A. Kurniawan, T. Juhana, and B. Ai, "Tabu-search-based pilot assignment for cell-free massive MIMO systems," *IEEE Trans. Veh. Tech.*, vol. 69, no. 2, pp. 2286–2290, 2019.
- [26] Y. Jin, J. Zhang, S. Jin, and B. Ai, "Channel estimation for cell-free mmWave massive MIMO through deep learning," *IEEE Trans. Veh. Tech.*, vol. 68, no. 10, pp. 10325–10329, 2019.
- [27] Z. Chen and E. Björnson, "Channel hardening and favorable propagation in cell-free massive MIMO with stochastic geometry," *IEEE Trans. Commun.*, vol. 66, no. 11, pp. 5205–5219, 2018.
- [28] T.-H. Tai, W.-H. Chung, and T.-S. Lee, "A low complexity antenna selection algorithm for energy efficiency in massive mimo systems," in *IEEE Int. Conf. Data Science and Data Intensive Systems*, 2015, pp. 284–289.

- [29] Z. Liu, W. Du, and D. Sun, "Energy and spectral efficiency tradeoff for massive MIMO systems with transmit antenna selection," *IEEE Trans. Veh. Tech.*, vol. 66, no. 5, pp. 4453–4457, 2016.
- [30] X. Gao, L. Dai, and A. M. Sayeed, "Low RF-complexity technologies to enable millimeter-wave MIMO with large antenna array for 5G wireless communications," *IEEE Commun. Mag.*, vol. 56, no. 4, pp. 211–217, 2018.
- [31] A. Kaushik, J. Thompson, E. Vlachos, C. Tsinos, and S. Chatzinotas, "Dynamic RF Chain Selection for Energy Efficient and Low Complexity Hybrid Beamforming in Millimeter Wave MIMO Systems," *IEEE Trans. Green Commun. Networking*, vol. 3, no. 4, pp. 886–900, 2019.
- [32] O. El Ayach, S. Rajagopal, S. Abu-Surra, Z. Pi, and R. W. Heath, "Spatially sparse precoding in millimeter wave MIMO systems," *IEEE Trans. Wireless Commun.*, vol. 13, no. 3, pp. 1499–1513, 2014.
- [33] A. Alkhateeb, O. El Ayach, G. Leus, and R. W. Heath, "Channel estimation and hybrid precoding for millimeter wave cellular systems," *IEEE J. Sel. Topics Signal Process.*, vol. 8, no. 5, pp. 831–846, 2014.
- [34] E. Viterbo and J. Boutros, "A universal lattice code decoder for fading channels," *IEEE Trans. Inf. Theory*, vol. 45, no. 5, pp. 1639–1642, 1999.
- [35] N. T. Nguyen, K. Lee, and H. Dai, "QR-Decomposition-Aided Tabu Search Detection for Large MIMO Systems," *IEEE Trans. Veh. Technol.*, vol. 68, no. 5, pp. 4857–4870, 2019.
- [36] N. T. Nguyen and K. Lee, "Groupwise Neighbor Examination for Tabu Search Detection in Large MIMO systems," *IEEE Trans. Veh. Technol.*, vol. 69, no. 1, pp. 1136–1140, Jan. 2020.
- [37] S. Han, I. Chih-Lin, Z. Xu, and C. Rowell, "Large-scale antenna systems with hybrid analog and digital beamforming for millimeter wave 5G," *IEEE Commun. Mag.*, vol. 53, no. 1, pp. 186–194, 2015.
- [38] Y.-Y. Lee, C.-H. Wang, and Y.-H. Huang, "A hybrid RF/baseband precoding processor based on parallel-index-selection matrix-inversion-bypass simultaneous orthogonal matching pursuit for millimeter wave MIMO systems," *IEEE Trans. Signal Process.*, vol. 63, no. 2, pp. 305–317, 2015.
- [39] T. S. Rappaport, G. R. MacCartney, M. K. Samimi, and S. Sun, "Wideband millimeter-wave propagation measurements and channel models for future wireless communication system design," *IEEE Trans. Commun.*, vol. 63, no. 9, pp. 3029–3056, 2015.
- [40] T. S. Rappaport, E. Ben-Dor, J. N. Murdock, and Y. Qiao, "38 GHz and 60 GHz angle-dependent propagation for cellular & peer-to-peer wireless communications," in *IEEE ICC*, 2012, pp. 4568–4573.
- [41] F. Sohrabi and W. Yu, "Hybrid digital and analog beamforming design for large-scale antenna arrays," *IEEE J. Sel. Topics Signal Process.*, vol. 10, no. 3, pp. 501–513, 2016.
- [42] X. Gao, L. Dai, S. Han, I. Chih-Lin, and R. W. Heath, "Energy-efficient hybrid analog and digital precoding for mmWave MIMO systems with large antenna arrays," *IEEE J. Sel. Areas Commun.*, vol. 34, no. 4, pp. 998–1009, 2016.
- [43] K. Roth and J. A. Nossek, "Achievable rate and energy efficiency of hybrid and digital beamforming receivers with low resolution ADC," *IEEE J. Sel. Areas Commun.*, vol. 35, no. 9, pp. 2056–2068, 2017.
- [44] K. Roth, H. Pirzadeh, A. L. Swindlehurst, and J. A. Nossek, "A comparison of hybrid beamforming and digital beamforming with low-resolution ADCs for multiple users and imperfect CSI," *IEEE J. Sel. Topics Signal Process.*, vol. 12, no. 3, pp. 484–498, 2018.
- [45] R. Méndez-Rial, C. Rusu, N. G. Prelcic, A., and R. W. Heath Jr, "Hybrid MIMO architectures for millimeter wave communications: Phase shifters or switches?" *IEEE Access*, vol. 4, no. 8, pp. 247–267, 2016.
- [46] A. Alkhateeb, G. Leus, and R. W. Heath, "Limited feedback hybrid precoding for multi-user millimeter wave systems," *IEEE Trans. Wireless Commun.*, vol. 14, no. 11, pp. 6481–6494, 2015.
- [47] T. E. Bogale, L. B. Le, A. Haghighat, and L. Vandendorpe, "On the number of RF chains and phase shifters, and scheduling design with hybrid analog-digital beamforming," *IEEE Trans. Wireless Commun.*, vol. 15, no. 5, pp. 3311–3326, 2016.